Development of a Novel Process to Fabricate Hierarchical Microporous Open-Cell Polymer Foam

By

Michael C. Fechtmann

A thesis submitted to the

Graduate School - New Brunswick

Rutgers, The State University of New Jersey

In partial fulfillment of the requirements

For the degree of

Master of Science

Graduate Program in Mechanical and Aerospace Engineering

Written under the direction of

Professor Shahab Shojaei-Zadeh

and approved by

_____

_____

_____

_____

New Brunswick, New Jersey

October, 2013

ABSTRACT OF THE THESIS

Development of a Novel Process to Fabricate Hierarchical Microporous Open-Cell Polymer Foam

by MICHAEL C. FECHTMANN

Thesis Director:

Professor Shahab Shojaei-Zadeh

A new process to fabricate polymeric hierarchical microporous foams was developed and the effects of process parameters on the cell structure, Young's Modulus, ultimate tensile strength and density of the resulting foams were studied. The process uses a suspo-emulsion in which one phase is volatile blowing agent/particle slurry and the other phase is a heat curable polymer. We found that the initial concentration of each of the components had drastic effects on the stability of the suspo-emulsion and whether or not the suspo-emulsion would phase invert to create polymer particles instead of polymer foam. Also, increasing the amount of blowing agent in a given suspo-emulsion resulted in lower density foam with a larger Young's modulus and higher ultimate tensile strength. Polydimethylsiloxane (PDMS) was the polymer chosen for the systematic study of the process and epoxy resin was also used to demonstrate the versatility of the process. Since the resulting foam is microporous and open-celled and because PDMS is hydrophobic, the produced foam rejects high surface tension liquids like water, but absorbs low surface tension liquids like motor oil. Thus, foams fabricated from different compositions were evaluated for their ability to absorb oil for their potential application in maritime oil spill cleanup operations.

Acknowledgements

First and foremost, I would like to thank my advisor, Dr. Shahab Shojaei-Zadeh for allowing me to conduct research under his watchful eye while still giving me the freedom to follow my interests. Admittedly, my focus waivered at times, but he was always there to guide me back. I will honestly miss the weekly research group meetings conducted by Professor Zadeh and I doubt I will get to experience another open exchange of ideas quite like those meetings ever again. I would also like to thank my thesis committee members, Dr. Alberto Cuitino and Dr. F. Javier Diez for the time they spent reviewing my thesis.

Professor Javier Diez and his students (especially Dan Piwowar) were of great help through the course of my research, and I cannot thank them enough. Professor Joseph W. Freeman and his student Brittany Taylor helped research potential biomedical applications for my project, which I could not have done on my own. I also want to thank my lab mates for their companionship and insightful discussions: Hossein Rezvantalab, Matt Ambrush, Ben Chung-Hsuan Huang, Matt Thorn, Stephen Rowe, Jeff Infante, Grace Choi, Sanath Sambamoorthi and Jordan Zuber. The lab was always buzzing with their presence and without them, my breadth of knowledge would be considerably less. John Petrowski and Joe Vanderveer helped me with technical and resource challenges often, and without their help the pace of my research would have been considerably slower.

My parents, Robert and Elise, supported and nudged me through my entire time at Rutgers, and I am forever indebted to them for their kindness. My brothers, Bobby and

Kurt, have barraged me with questions and ideas (and absurdities), all of which I am very thankful for. I would like to thank my girlfriend, Alison Anuzis, and the rest of the Anuzis clan for listening to my ramblings and taking interest in my work. Last but not least, I would like to thank my friends for not letting me work too hard and for helping me to see the science behind the mundane. They are: Dan Piwowar, Pinto Adhola, Troy Buckley, Brian Parsons, Andrew Chen, Danny Etherton, Elesha Kasimir, Raquel Palacios, Andrea Kopanja, Katya Belakovskaya, Megan Wiseman, Kalyan Yalamanchi, Joshua Hoff, Bharat Chandrasekaran, William Grier, Lane Outz, and Vincent Marotti.

Michael C. Fechtmann

Rutgers, The State University of New Jersey

June 18, 2013

Table of Contents

List of Figures

distinct end products depending on the concentrations of isopropanol and sugar. The end product of interest in the systematic study is the open-cell foam. The inset image is a micrograph of PDMS particles (scale bar 300μm) generated from the phase inverted section of the phase diagram.

Figure 10. FE-SEM micrographs of a sample of foam before the sugar is dissolved. It is clear that the sugar is pushed together by the expanding isopropanol bubbles and that the sugar lies between films of PDMS.

Figure 11. Selected time laps images of thin films made from mixtures of only two of the three required components: (a) PDMS/Sugar, (b) Sugar/Isopropanol, (c) Isopropanol/PDMS. Image (d) represents the sample where all three required components (PDMS/Isopropanol/Sugar) are present. All scale bars are 200 microns.

Figure 12. Normalized bubble growth of 1mm thick films of the suspo-emulsion at 25°C. Increasing isopropanol or reducing sugar concentration leads to faster bubble growth. The data is fitted to quadratic curves with the displayed R^2 values.

Figure 13. Normalized bubble growth of 1mm thick films of the suspo-emulsion at 38°C. A larger concentration of sugar has a more dramatic negative effect on the bubble size at an elevated temperature. The data is fitted to quadratic curves with the displayed R^2 values.

Figure 14. FE-SEM micrographs of the cross section of foams prepared using a composition of 1.86g/mL isopropanol, 4.12g/mL sugar and 4.85mL PDMS at different curing temperatures. (b) is an example of mesoscale pores that can be found in these foams. All scale bars are 200 microns, except for (b) which has a scale bar that is 2 microns.

Figure 15. FE-SEM micrographs of foams that all have 1.44g/mL of isopropanol and 4.85mL of PDMS, with various sugar concentrations. As the sugar concentration is increased, the foam morphology becomes dominated by pores resulting from the dissolution of sugar. All scale bars are 200 microns.

Figure 16. FE-SEM micrographs of foams that all have 5.15g/mL of sugar and 4.85mL of PDMS with different isopropanol concentrations. As the isopropanol concentration is increased the foam morphology becomes dominated by large pores formed by isopropanol bubbles. All scale bars are 200 microns. (b) is a close up of the structure shown in (a).

Figure 17. Schematic of the setup for determining the density of the foam samples. An anchor weight of known volume was attached to the foam sample and then placed in a graduated cylinder. The cylinder was then filled with water to a predetermined graduation. The difference between the weight of water and the graduation is the volume occupied by the foam sample and the anchor weight.

Figure 18. A plot of the density of the foams as a function of the sugar concentration. Changing the isopropanol concentration in the suspo-emulsion has a more drastic effect on the density at higher sugar concentrations, showing that the density is an interdependent function of sugar and isopropanol. The data is fitted to exponential decay functions with the displayed R^2 values.

Figure 19. The effect of isopropanol concentration on foam density. The density is inversely proportional to the isopropanol concentration for a given sugar concentration. The data is fitted to lines with the displayed R^2 values.

Figure 20. The influence of sugar concentration on the porosity (calculated from the density) of the produced foams. The porosity is proportional to the sugar concentration but at higher sugar concentrations the isopropanol concentration creates greater variation. The data is fitted to quadratic curves with the displayed R^2 values.

Figure 21. Pore size distribution generated from SEM micrographs for foam samples fabricated with a constant isopropanol concentration of 1.44g/mL. There is a wide distribution of pore sizes and the highest sugar concentration has the greatest number of pores in each bin except for the 10^2 bin.

Figure 22. Average pore area generated from SEM micrographs of foam samples fabricated with a constant isopropanol concentration of 1.44g/mL. The average pore area decreases with an increase in the sugar concentration. The data is fitted to a line with an R^2 value of 0.84125.

Figure 23. Pore area standard deviation generated from SEM micrographs of foam samples fabricated with a constant isopropanol concentration of 1.44g/mL. The standard deviation of the pore area decreases with an increase in the sugar concentration, indicating that the pores become more uniform in size. The data is fitted to a line with an R^2 value of 0.82992.

Figure 24. Porosity of foam samples calculated from their densities**.** The porosity of the foam sample is proportional to the isopropanol concentration. There is a comparatively large jump in porosity between the samples prepared with sugar concentration of 2.06g/mL and 3.09g/mL. The data is fitted to lines with the displayed R^2 values.

Figure 25. Pore size distribution generated from SEM micrographs of foam samples prepared with a constant sugar concentration of 5.15g/mL**.** A lower isopropanol concentration will lead to more pores in the 10^3 micron^2 bin.

Figure 26. Average pore area generated from SEM micrographs of foam samples fabricated with a constant sugar concentration of 5.15g/mL. The average pore area increases with an increase in the isopropanol concentration. The data is fitted to an exponential equation with an R^2 value of 0.97827.

Figure 27. Pore area standard deviation generated from SEM micrographs of foam samples fabricated with a constant sugar concentration of 5.15g/mL. The standard deviation of the pore area increases with the isopropanol concentration, indicating that the pores become less uniform with an increase in the isopropanol concentration. The data is fitted to a line with a R^2 value of 0.90015.

Figure 28. An example of a graph of the raw data from the Instron tensile test machine. Foam samples were tested until failure. The UTS is the peak values of stress attained before sample failure.

Figure 29. Average of three Ultimate Tensile Strength (UTS) tests for each of the foam compositions. The UTS of the foam samples increases with increasing isopropanol concentration, but decreases with the addition of sugar. The UTS of bulk PDMS is 2.24MPa. The data is fitted to exponential functions with the displayed R^2 values.

Figure 30. Groups of samples with a constant sugar concentration (in g/mL) are circled. Within each of these groups an increase in the isopropanol concentration not only leads to a decrease in the density of the foam, but also to an increase in the UTS.

Figure 31. Average of the Young's Modulus of three samples for each composition**.** The Young's Modulus of the foam will increase drastically with an increase in the isopropanol concentration when there is a low sugar concentration in the suspo-emulsion, but when there is a higher concentration of sugar in the suspo-emulsion, the isopropanol concentration has less of an effect. The Young's Modulus of bulk PDMS ranges from 360KPa to 870KPa. The data is fitted to quadratic equations with the displayed R^2 values.

Figure 32. Groups of samples with constant sugar concentrations (in g/mL) are circled. Within each of these groups, an increase in the isopropanol concentration leads to a lower density, but also a higher Young's Modulus. The effect becomes less significant at higher sugar concentrations.

Figure 33. Normalized mass gains for foam samples placed on top of oil slick for 1 minute**.** Generally**,** more oil is absorbed by foam samples that were fabricated with higher isopropanol and sugar concentrations. The data is fitted to quadratic equations with the displayed R^2 values.

Figure 34. Normalized mass gains for foam samples placed on top of oil slick for 15 seconds**.** Oil absorption after 15 seconds shows a similar trend to the 1 minute experiment, but the normalized mass gains are lower. The data is fitted to cubic equations with the displayed R^2 values.

Figure 35. Normalized mass gains for foam samples placed on top of oil slick for 1 minute plotted against the density. The normalized mass gains appear inversely proportional to the density of the foam samples. Inset (a) is a picture of the foam before

List of Tables

List of Symbols

Symbol	Description	Units
A_0	Initial Area	μm^2
A_n	Normalized Area	A.U.
A_t	Area at time t	μm^2
E	Young's Modulus	kPa
F	Force	N
L_0	Initial Length	cm
ΔL	Change in Length	cm
ε	Tensile Strain	A.U.
ρ_s	Density of a Foam Sample	g/cm^3
ρ_w	Density of Water	g/cm^3
σ	Tensile Stress	Pa
V_a	Volume of Anchor	cm^3
V_g	Volume as Read on Graduated Cylinder	cm^3
V_s	Volume of a Foam Sample	cm^3
M_f	Final Mass	g
M_i	Initial Mass	g
C_{IPA}	Concentration of Isopropanol (IPA)	g/mL
M_s	Mass of a Foam Sample	g
C_{SU}	Concentration of Sugar	g/mL
M_w	Mass of Water	g
MG	Mass Gain	A.U.

Chapter 1

Introduction

1.1 Polymer Foam Background

In this study we have developed a novel method of foaming a liquid pre-polymer matrix which is then crosslinked into a solid and hierarchically structured open-cell foam. Open-cell foams have many applications, including bioscaffolds[1-3], high surface area catalysts[4, 5], filters[6], battery, capacitor and fuel cell electrodes [7, 8], vibration/acoustic dampers[9, 10], thermal insulation[11, 12], and sorbents[13, 14]. Polymeric open-cell foams are of particular interest due to their relatively low cost, low weight and wide range of physical and mechanical properties. There are four basic mechanisms of manufacturing polymer foams: gaseous blowing agents, liquid blowing agents, emulsion templating and porogen (a solid particulate pore generator) leaching. Schematics for these mechanisms are presented in Figure 1. These mechanisms can produce both open and closed cell foams, with the transition between the two structures relying upon the percentage of void space created in the particular foam[15]. Each of the basic mechanisms can be broken down into a variety of specific methods, for example, a gaseous blowing agent can be physically blown/injected into a viscous polymer and then heated to expand into pores, or gas molecules could be a byproduct of the polymerization reaction and collected into bubbles that become the cells of the foam[16]. A blowing agent that does not undergo a chemical reaction during the foaming process is termed a physical blowing agent, whereas chemical blowing agents are gasses created from a chemical reaction. Of course, each of these methods has its advantages and drawbacks. Gas bubbles (or liquid droplets) generated by gaseous blowing agents, liquid blowing agents and emulsion templates need to be stabilized (usually with a surfactant) to prevent their coalescence so that large voids do not occur in the final polymer foam. The bubbles/droplets in these three methods can also be stabilized by low surface energy

particles at the bubble (or droplet) interface or by both particles and surfactants. An example of an emulsion templated foam that is stabilized by both particles and surfactants, and results in the formation of a hierarchical pore structure is shown in Figure 2. The small pores are due to surfactant stabilized droplets and larger pores are due to particle stabilized droplets[17]. A hierarchical pore structure – a mixture of pore sizes of different length scales, i.e. a mixture of micropores (diameter 1μm to 1mm) and macropores (diameter >1mm), gives foams improved absorption capabilities over uniform cell size foams due to the differing transport rates of fluids through large and small pores in the foam's structure[18], as well as improved mechanical properties[19].

Porogen leaching methods generally do not have to be stabilized, but the solid porogen must be removed from the polymer matrix, which can be a cumbersome and wasteful process, especially as the size of the porogen (and hence pores of the foam) is reduced. However, templating and subsequent leaching of solid fillers is one of the simplest and most robust techniques for creating open-cell structures. Common solid porogens include sugar (sucrose)[20-30] and salt (sodium chloride)[23, 28-40] because they are easily dissolved in water, as opposed to polymeric porogens that require the use of organic solvents for dissolution. Ice has also been shown to be an effective solid porogen[41-43], as it can easily be melted away.

There are other more exotic methods of creating polymer foams, such as using micelles to create the pores of the foam [44, 45] or by stabilizing aqueous foams solely by polymer particles at the liquid-gas interface and then sintering the polymer particles into one solid structure (see Figure 3) [46-49].

As there are many methods of creating polymer foams, foams are also created from many different types of polymers with a wide range of properties. Foams are made from

thermoplastic and thermoset polymers, biopolymers, hydrophobic and hydrophilic polymers and elastomers. Commonly foamed polymers include polystyrene (especially for consumer food containers), polyurethane, polyvinylchloride, polypropylene, polyethylene and silicone.

Silicone open-cell foams are of particular interest because they have been shown to be able to separate oil from water due to the inherent hydrophobicity and oleophilicity of silicone[22]. This property coupled with a high chemical resistance, a low glass transition temperature (-125ºC) and stability at high temperatures[50] make silicone foams the ideal candidate for cleaning up oil spills in harsh environments. Not only are the physical properties of the silicone foam important, but so is the morphology of the cellular structure. Recently there has been much interest in creating hierarchical pore morphologies in foams[51-60] due to their improved mechanical and physical properties. Creating a hierarchical structure requires a combination of the methods outlined previously or using multiple sizes of the same type of template.

In this study we have developed a novel method that is a combination of porogen leaching and liquid blowing agent methods to create hierarchical silicone foam. The porogen particles are mixed into the blowing agent to create a suspension that is then emulsified with the pre-polymer/curing agent mixture to create a suspo-emulsion (an emulsion in which one of the phases is a suspension). Upon heating, the blowing agent expands to create bubbles and the pre-polymer is solidified. Finally, the porogen particles are dissolved away. This method is unique in that the suspo-emulsion from which the foam is produced is stabilized not by particles at the interface or by surfactants, but by the increase in viscosity from the addition of particles in the bulk of the blowing agent phase. Thus, low surface energy (generally polymeric) particles are not required for this

technique, nor are surfactants, both of which can be environmentally hazardous if they were to leach out of the foam. From the perspective that this method is essentially adding a blowing agent to the conventional porogen leaching method, one can see that the blowing agent helps to create a continuous network for the porogens to be leached from at much lower porogen concentrations. From the other perspective, that this method is adding porogens to the conventional liquid blowing agent process, one can see that the viscosity of the lower molecular weight polymers can be modified with porogens to trap liquid blowing agents. Additionally, the removal of the porogen particles and the expansion of the blowing agent leads to a hierarchical pore structure that can be controlled by the concentrations of the blowing agent and porogen.

1.2 Motivation

We are seeking a process-structure-property relationship for a novel method of creating hierarchical foams and to determine if any of the resulting foam compositions are viable for cleaning maritime oil spills. The novel process will be shown to create foams from two different polymers, and with two different fillers. The process can run into difficulties such as phase separation if the concentration of the starting components are in improper proportions, so a processing window (or phase diagram) needed to be determined. This phase diagram also gives insights into the interesting physics of the process.

1.3 Thesis Outline

First, the production process and the materials used in the process will be explicitly stated. The phase diagram for the selected materials and temperature will be explained, as will the physics behind the process. The effect of the concentrations of the components in the pre-foamed mixture on the resulting mechanical and physical properties of the final

foam, along with their testing methods, will be explained. Lastly, the potential application of the produced foam for maritime oil spill cleanup will be examined.

Chapter 2

Process Development

2.1 Production Process

A flow diagram of the production process is shown in Figure 4. First, a given mass of powdered sugar (the porogen/filler) is weighed into a container on a milligram scale (Mettler Toledo), followed by the addition of a given mass of isopropanol (the liquid blowing agent). These two components are then mixed by hand for 30 seconds, and then mixed in a high shear centrifugal mixer (Thinky AR-100) at 2000 RPM for 1 minute to create the blowing agent/filler slurry forming the inner phase of the suspo-emulsion. In a separate container, a mixture of PDMS elastomer base and crosslinker is prepared with the components in a 10:1 ratio, respectively. This combination is mixed by hand for 30 seconds, and then mixed in the high shear centrifugal mixer at 2000 RPM for 1 minute. This mixture becomes the outer phase of the suspo-emulsion, and thus, the foam. Next, 4.85mL of the PDMS base/crosslinker mixture is added into the isopropanol/sugar slurry to create the precursor to the blowing agent slurry/polymer suspo-emulsion. The final slurry/polymer suspo-emulsion is created by mixing the precursor mixture for 1 minute by hand and 2 minutes at 2000 RPM in the centrifugal mixer. Additionally, the suspo-emulsion is de-foamed in the centrifugal mixer for 1 minute to remove air bubbles that are entrained during mixing and to ensure as homogeneous of a foam as possible.

The suspo-emulsion is then placed in the oven at a given temperature for 1 hour to crosslink (cure) the PDMS and to cause the liquid isopropanol to vaporize into bubbles. After curing, slight and variable compression is applied to the foam while under a stream of water to help the water infiltrate the pores of the foam to aid in dissolving the sugar particles. The samples are then placed in a container of water for 12 hours to ensure the removal of all the sugar particles. The samples are then dried in an oven for 4 hours at 80°C resulting in the formation of the final foam structure. Three parameters were

systematically varied in this study in order to determine their influence on the structure and the mechanical properties of the resulting foams: isopropanol, powdered sugar, and the curing temperature. Figure 5 is a schematic of the process after the suspo-emulsion has been made. During the heat curing process the isopropanol expands into bubbles that are trapped by the PDMS. These isopropanol vapor bubbles push the sugar to their edges to create a continuous network of sugar through the PDMS. Once the sugar is dissolved, the PDMS hierarchical foam structure is released.

2.2 Equipment

Disposable containers that were chemically resistant to isopropanol and had melting temperatures well above 80°C were used to contain the mixtures and emulsions that resulted from the various stages of the production process. The foam was produced in 90mL polystyrene cups and in 22mL glass vials. A Mettler Toledo scale with a milligram resolution was used to weigh the components into the container. A mini stainless steel spatula was used to mix the components by hand and a Thinky AR-100 centrifugal mixer was used to mix, de-foam and emulsify the components. A convection oven was used to heat the final emulsion to cure the polymer and vaporize the blowing agent.

2.3 Materials Selection

Polydimethylsiloxane (PDMS) was purchased in the form of the Sylgard 184 elastomer base and crosslinker kit (Dow Corning) and was used as the polymer matrix of the foam in this study. PDMS was selected because it can be cured in a wide temperature range, allowing the blowing agent to be tested at several different temperatures. Polyepoxide 635 thin epoxy resin and hardener (US Composites, Inc.) was used as an alternate polymer matrix to show the versatility of the foaming method and to demonstrate that the process can be used with different types of polymers. Figures 6(a-c)

show a field emission scanning electron microscope (FE-SEM) image of a foam made using this process with 4.85mL of epoxy resin, 3.09g/mL of sugar and 1.02g/mL of isopropanol. It shows a similar structure to PDMS foam with a high loading of sugar and a low loading of isopropanol (see Figure 16 (a)). Domino Sugar 10-X powdered confectioners' sugar (Domino Foods, Inc.) was used as the solid filler (porogen) for the systematic study. Powdered sugar was used because it is easily dissolved away in water after curing and because it is only slightly soluble in isopropanol which allows slurries to be made at relatively low sugar concentrations as compared to water. An FE-SEM image of the powdered sugar is shown in Figure 7.

The powdered sugar was run through 75 micron mesh at the Domino production factory, so that is the maximum particle size. Sodium bicarbonate (Church & Dwight Co., Inc.) and sodium chloride (Morton Salt) were also used to show that this method is compatible with multiple solid fillers. These solid fillers also have low solubility in isopropanol, which allows thick slurries to be made at low filler concentrations. Figures 8(a-b) are FE-SEM micrographs of the PDMS foam with sodium bicarbonate as the filler. The hierarchical structure of the foam is demonstrated in these images.

For the liquid blowing agent, 70% isopropanol (TopCare) was used as it does not interfere with the curing reactions of PDMS and polyepoxide. Distilled water was used to remove the solid filler from the foam after curing. For the oil absorption tests, Mobil Special SAE 5W-30 motor oil (Exxon Mobil Corporation) with a density of 0.86g/mL was used.

2.4. Process Temperature

The foaming process is highly temperature dependent because the rate of curing of

the PDMS and the rate of vaporization of the isopropanol are both temperature dependent. Therefore, the interplay of these two dynamic parameters is very important to the resulting foam. It stands to reason that the faster the PDMS cures, the less time the isopropanol has to vaporize and expand. The standard curing temperature of PDMS is 65°C and the boiling point of 70% isopropanol/30% water is 80.4°C, so they are within approximately 15°C of each other. A solution of 70% isopropanol/30% water forms an azeotrope (a mixture of two liquids that has a single boiling point), so the separation of water and isopropanol will not occur during the vaporization process.

2.5 Phase Diagram

The percentage of the liquid PDMS phase versus the percentage of the sugar in isopropanol suspension phase is very important to the structure of this emulsion. An increase in the percentage of the inner phase (the sugar in isopropanol suspension) can cause phase inversion, which is the inner phase becoming the outer phase. Conversely, a reduction in the percentage of the outer phase (the liquid PDMS) can also cause phase inversion. If the emulsion is unstable, then phase separation can occur and the inner phase and outer phase will separate and stack by density in the container (PDMS on top of sugar/isopropanol). Since one of the phases of this emulsion is a suspension of particles in a liquid, it is a type of emulsion termed suspo-emulsion.

A phase diagram for the PDMS/sugar/isopropanol suspo-emulsion is shown in Figure 9. For each of the compositions in the phase diagram the volume of PDMS was held constant at 4.85mL with the base to crosslinker ratio held constant at 10:1. Additionally, the curing temperature was held constant at 80°C (approximately the boiling point of the 70% isopropanol/30% water azeotrope). At the bottom left hand corner of the phase diagram there is a low concentration of sugar and a low concentration of isopropanol and

in this region a closed cell foam results after curing. It is difficult to dissolve any of the sugar out of the foam in this region. Increasing the sugar concentration without increasing the isopropanol concentration brings the system into a region where an open cell foam results after curing, but the structure is extremely weak and the foam crumbles apart when the sugar is dissolved away. Increasing the isopropanol concentration from this point brings the system to the center of the phase diagram, where an open-cell hierarchical foam is formed after curing. This was the main region of interest for this study, with the PDMS as the outer phase of the emulsion and sugar/isopropanol as the inner phase. Increasing the concentration of isopropanol from this region brings the system into the phase separation region, in which the isopropanol and sugar migrate to the bottom of the container and the PDMS migrates to the top during the curing process. Increasing the sugar concentration from this region can bring the system back into the stable zone where the open-cell hierarchical foam is produced. Increasing the concentration of sugar even further will push the system to a phase inversion point, causing the PDMS to become the inner phase of the emulsion and sugar/isopropanol to become the outer phase of the emulsion. PDMS particles are created after curing when the system is in this region, as seen in the inset image in Figure 9.

It is interesting to note that the addition of sugar prevents phase separation from occurring, while the addition of isopropanol can cause phase separation. It stands to reason that the sugar particles in the bulk are stabilizing the system because the addition of particles will increase the viscosity of the isopropanol/sugar phase (which is clearly noticeable during mixing). Additionally, the thinning effect of adding more isopropanol causes the suspo-emulsion to become less stable. The stability of a specific composition of the suspo-emulsion can be predicted by the equation that forms the line separating the

phase separation region from the open cell foam region of the phase diagram in Figure 9, as:

$$C_{IPA} = 0.83C_{SU} - 0.34 \quad (1)$$

Where C_{IPA} is the concentration of isopropanol and C_{SU} is the concentration of sugar. This equation will give the maximum isopropanol concentration that can be used for a given sugar concentration without phase separation, when the temperature is 80°C. The equation for the lower bound where foams begin to crumble apart is:

$$C_{IPA} = 0.23C_{SU} - 0.16 \quad (2)$$

This equation will give the maximum sugar concentration that can be used for a given isopropanol concentration without causing the foam to crumble, when the processing temperature is set to 80°C. These two equations are only valid between sugar concentrations of ~0.5g/mL, where closed cell foams results, and ~9g/mL, which is where phase inversion will start to occur. FE-SEM micrographs of the foam before the sugar was dissolved away are shown in Figures 10(a-c). The sugar particles tend to form interconnected granules that help create the open cell structure of the foam. The film of PDMS that formed around the sugar is also clearly visible.

2.6 Bubble Growth

The pre-cured mixture was produced following the procedure detailed in Section 2.1. A one millimeter thick film of the mixture was doctor blade extruded onto a glass slide. This film was viewed from the bottom (through the glass slide) on an Olympus IX71 inverted microscope and a time lapse video was taken over the course of 20 minutes, with a picture taken every 30 seconds. A thermocouple was used to measure the temperature of the mixture on the slide. To extract data from the images, a color threshold was performed to isolate the bubbles from the background, and then the areas of three bubbles

were measured in each picture of the time lapse using the image processing program ImageJ. With these measurements, the area of each bubble was normalized by the formula:

$$A_n = \frac{A_t}{A_0} - 1 \quad (3)$$

Where, A_n is the normalized area, A_t is the area at time t, and A_0 is the area of the bubble at time $t = 0$, which corresponds to one minute after the emulsion was removed from the mixer. Using this normalization scheme the average bubble growth was compared for three bubbles in four different compositions of sugar and isopropanol and at two different temperatures. The glass slide was heated with a resistive heating element in contact with the slide.

To confirm that the isopropanol was expanding and creating bubbles during the foaming process, two of the three components (isopropanol, PDMS, and sugar) were selected and a mixture was made. This was repeated for all possible combinations: isopropanol/PDMS, isopropanol/sugar and PDMS/sugar using the same procedure outlined in Section 2.1, though without one of the components. A time lapse video was taken as described previously.

From the experiments where one of the three components (isopropanol, PDMS, and sugar) was removed from the mixture, it is clear that all of them together are necessary to create the foam structure. The mixture of just PDMS and sugar created no bubbles, as was expected due to the lack of the volatile isopropanol. The mixture of isopropanol and sugar did not create any bubbles either, which was also expected due to the lack of a continuous matrix to house the bubbles. The mixture of isopropanol and PDMS did form bubbles, however, there were very few compared to when all three components were in

the mixture. Figures 11(a-d) show representative images from the time lapse of these three mixtures compared to a mixture where all three components exist.

Four compositions were tested for emulsions that contained all three components. The average normalized bubble size versus time for each composition at 25˚C and at 38˚C are shown in Figure 12 and Figure 13, respectively.

To analyze the growth rate of the bubbles, a quadratic equation was fit to each of the curves, and the first derivative of that quadratic equation was taken as the bubble growth rate. The coefficient of the first order term of the first derivative is negative in for all compositions and represents the factors that slow down the bubble growth rate as time progresses. These factors include the dissipation of vaporized isopropanol into the atmosphere and the increase in the viscosity of PDMS as the polymer chains are crosslinked. The zeroth order coefficient (constant) of the first derivative represents the factors that do not change with time, such as the initial concentrations of isopropanol and sugar and the temperature of the glass slide. At 25°C and a concentration of 3.09 g/mL of sugar, an increase in the concentration of isopropanol by 50% results in an decrease of the coefficient of the first order term of the slope by 1250% and of the constant term by 144%. This physically means that a 50% higher isopropanol concentration initially increases the bubble growth rate by 144%, but as time progresses the bubble growth rate tapers off 1250% more quickly. Table 1 provides the compositions that were evaluated and the first and zeroth order coefficients for each of the compositions at 25°C and 38°C.

Generally, for the compositions that were evaluated, a lower concentration of sugar results in an increased bubble growth rate, which is likely due to the reduced viscosity of the suspo-emulsion. A higher concentration of isopropanol also results in an increased bubble growth rate, which could be due to a decrease in the viscosity of the suspo-

emulsion and/or more isopropanol available for vaporization. The change from 25˚C to 38˚C results in an increase in the bubble growth rate for all compositions because the liquid isopropanol expands as it vaporizes into a gas. We anticipate that the same factors that increase the bubble growth rate in the evaluation of these foam films will also increase the bubble growth rate in a bulk foam, and thus lead to a lower density bulk foam.

Chapter 3

Physical and Mechanical Properties

3.1 Morphology

Analysis of the morphology of the resulting foam is essential in determining the variables that affect the production process of the foam. Additionally, there is a three way relationship between processing, structure, and properties of a material, and to fully understand a material system, the relationship between all three must be determined. In this study three variables were shown to greatly influence the morphology (and thus the material properties): curing temperature, sugar concentration, and isopropanol concentration. All experiments from this point on were performed in the open-cell foam region of the phase diagram (Figure 9).

FE-SEM micrographs were taken to compare the cell morphology of each of the foam samples. The samples were prepared for the FE-SEM using the freeze fracture technique. The foam samples were placed in liquid nitrogen for 1 minute to bring them below the glass transition temperature of PDMS. The samples became brittle, and were easily fractured. This freeze fracturing process allowed images of unadulterated foam to be taken, as normal cutting of foam results in damage to the pores of the foam. Since PDMS is an electrical insulator and the FE-SEM requires the surface of an object to be electrically conductive for proper imaging, all samples were sputter coated with a thin film of 25nm thick gold. All presented images are thus of the fractured and gold coated surfaces.

3.1.1 Effect of Curing Temperature

The curing temperature was varied from 50°C to 90°C in increments of 10°C. For these trials the composition of the foam was held constant with an isopropanol concentration of 1.03g/mL, a sugar concentration of 2.06g/mL and the volume of PDMS was 4.85mL. Figures 14(a-f) show the pore morphologies at each curing temperature. At

a curing temperature of 50°C it is apparent that the morphology of the foam is more heavily influenced by the pores formed from the sugar particles than pores formed from isopropanol bubbles. This is evidenced by the lack of many large cells formed from the expansion of the isopropanol.

In comparison to 50°C, the 60°C sample also shows cells formed from the expansion of the isopropanol, however, there are many more of these cells. There is not an appreciable difference between the sample prepared at 60°C and the sample prepared at 70°C as both display a similar pore structure. The samples prepared at 80°C and 90°C show more chaotic cell structures which are likely due to the rapid expansion of isopropanol and coalescence of the isopropanol bubbles. It is apparent that pores are formed by both mechanisms at every temperature that was evaluated, however, at 50°C the sugar particle have more influence on the structure than the isopropanol does, at 60°C and 70°C the influence of the isopropanol becomes more apparent, and at 80°C and 90°C the isopropanol causes a chaotic cell structure and the sugar particle voids are not as apparent as they were at the lower temperatures.

3.1.2 Effect of Sugar Concentration

For the set of images shown in Figures 15(a-d) the concentration of sugar was varied from 2.06g per milliliter of PDMS to 5.15g per milliliter of PDMS in 1.03g/mL increments, while the other parameters were held constant. The temperature was held at 80°C, the concentration of isopropanol in PDMS was held constant at 1.44g/mL and the volume of PDMS was held constant at 4.85mL. At a sugar concentration of 2.06g/mL the isopropanol appears to be the dominant pore generator, though there are smaller pores in the cell walls that are formed by the removal of the embedded particles of sugar. At a sugar concentration of 3.09g/mL there are clumps of sugar particles that surround the cell

walls generated by the isopropanol. PDMS also surrounds the clumps of sugar particles and thus, the dissolution of the sugar creates an array of PDMS cells created by isopropanol expansion that is connected by PDMS lamellae created around the sugar particles. This is comparable to foam formed from surfactant stabilized polymer emulsions, in which the polymeric outer phase forms films between domains of the liquid inner phase. However, the structure of the present foam is more complex because the inner phase is a suspension of particle in a volatile liquid. At a sugar concentration of 4.12g/mL the cells formed from isopropanol become less prevalent and the smaller chaotic cells formed by the sugar become more prevalent. This trend continues and at a sugar concentration of 5.15g/mL the cell structure is reversed as the sugar dissolution becomes the main pore generating mechanism.

3.1.3 Effect of Isopropanol Concentration

The set of images in Figures 16(a-f) displays the variation of the concentration of isopropanol from 1.03g/mL of PDMS to 1.86g/mL in ~0.20g/mL increments, while holding the temperature at 80°C, the concentration of sugar at 5.15g/mL of PDMS and the volume of PDMS at 4.85mL. When the concentration of isopropanol is 1.03g/mL the morphology of the foam is dominated by the relatively high concentration of sugar as it displays a fine structure caused by the dissolution of the sugar. There are very few cells formed from the expansion of the isopropanol in this case. As expected, increasing the concentration of isopropanol to 1.24g/mL resulted in increasing the number of cells formed by the expansion of isopropanol. The trend continues as the isopropanol concentration is increased to 1.44g/mL and 1.65g/mL with more lamellae between isopropanol cells forming as well. When the isopropanol concentration is 1.86g/mL the structure displays two interpenetrating networks of the pores formed by the two pore

generating methods. This trend is exactly the opposite of the trend shown previously in Figure 15 for increasing the sugar concentration.

3.2 Density of Fabricated Foams

The density of foams has been shown to greatly influence their mechanical properties, with higher density foams showing higher tensile and compressive strength and a larger Young's modulus. This should be fairly obvious to an observer, as a test sample of foam of the same volume as a solid sample will contain less material. However, not all foams are created equal and two foams with the same density but a different pore morphology (i.e. homogeneous vs. hierarchical) may have significantly different mechanical properties.

In this study, the density of the foam was simply determined by dividing the weight of a sample by its volume. The volume of the sample was determined by a water displacement technique. The setup for the water displacement is shown schematically in Figure 17. First, since the foam floats on top of water, the volume of an anchor needed to be determined. The sample was weighted down with an anchor in a graduated cylinder on top of a scale and the weight was tared. The foam is microporous and hydrophobic and, therefore, water cannot penetrate the foam under low pressure, so the graduated cylinder was filled with water to a predetermined volume graduation. The value of the volume graduation minus the volume of water gives the volume of the sample plus the weight. The formula to determine the volume of the sample from this process is as follows:

$$V_s = V_g - \frac{M_w}{\rho_w} - V_a \tag{4}$$

Where, V_s is the volume of the sample, V_g is the volume of the system as read on the graduated cylinder, M_w is the mass of the water as read on the scale, ρ_w is the density of

water, and V_a is the volume of the anchor used to keep the foam submerged. The density of the foam sample is simply:

$$\rho_S = \frac{M_S}{V_S} \tag{5}$$

Where, ρ_S is the density of the foam, M_S is the mass of the foam and V_S is the foam volume.

3.2.1 Influence of Sugar Concentration on Foam Density

To determine the effect that the sugar concentration has on the density of the foam, a matrix of foam samples with varying sugar and isopropanol concentrations were made in cylindrical vials. These samples were made with sugar concentrations that varied from 2.06g/mL to 5.15g/mL in 1.03g/mL increments and isopropanol concentrations that varied from 1.03g/mL to 1.86g/mL in 0.206g/mL increments. The volume of PDMS was held constant at 4.85mL. Of these 20 sample compositions, two were found to be unstable and phase separated. Both of these samples had isopropanol concentrations of 1.86g/mL (the highest tested) and sugar concentrations of 2.06g/mL and 3.09g/mL (the lowest and second lowest tested). Thus, there are no densities reported for these two compositions.

Since the sugar is eventually dissolved out of the foam, one would expect that a higher initial sugar concentration would result in lower foam density. This is exactly what is observed, however, the higher concentration of sugar may also result in the composition retaining more isopropanol, leading to further expansion, and thus a lower foam density. Apparently, there is also a competing effect from the increase in viscosity of the suspension (as evidenced by increased difficulty when hand mixing) due to the increased concentration of sugar and therefore the density-sugar concentration plot is

non-linear. Figure 18 is a plot of the sugar concentration versus the density of each of the resulting foams for each of the compositions. The grouping of the constant isopropanol curves at each interval is interesting to note because they tend to diverge as the amount of sugar is increased.

3.2.2 Influence of Isopropanol Concentration on Foam Density

To determine the effect of the isopropanol concentration on the density of the foam the same matrix of samples from the previous section was analyzed. Again, the isopropanol concentration was varied from 1.03g/mL to 1.86g/mL in 0.206g/mL increments while the concentration of sugar was varied from 2.06g/mL to 5.15g/mL in 1.03g/ml increments and the volume of PDMS was held constant at 4.85mL. Figure 19 is a plot of the density versus isopropanol concentration for each of the compositions. As the isopropanol concentration is increased, the density of the foam is decreased. This is in agreement with our observations in the bubble growth experiments where an increase in the isopropanol concentration resulted in a faster rate of bubble growth (see Table 1). Larger bubbles in the suspo-emulsion result in larger pores in the cured foam and thus a lower overall density. It is also interesting to note that in the density-isopropanol plot the constant sugar concentration best fit equations are linear as opposed to the curves in the density-sugar plot.

3.3 Porosity and Pore Size Distribution

The porosity of a foam is a measure of the void space in the foam, and for open cell foams such as those in this study, the porosity determines the maximum amount of fluid that can be held in the foam. The porosity is the opposite of the density; as density is a measure of the amount of material per unit volume and porosity is a measure of the amount of void space per unit volume. However, the porosity of the foam does not

provide information on the size of the pores in the foam. A measurement of the pore size distribution is required to determine the size of the pores in the foam. The pore size distribution is important in determining the degree of hierarchy of the pores and is a standard method to quantify the morphology of the foam. Foams that display a hierarchical structure have been shown to have improved mechanical properties over heterogeneous foams without a hierarchical structure[19].

The porosity of the foam was determined from Equation 6:

$$P = 1 - \frac{\rho_S}{\rho_{PDMS}} \tag{6}$$

Where P is the porosity of the sample, ρ_s is the measured density of the sample and ρ_{PDMS} is the density of cured PDMS (~1.03g/mL).

The pore size distribution was determined from the SEM micrographs. The micrographs were turned into binary black and white images using ImageJ, and then an algorithm to remove single pixel specks was used so that the Analyze Particles function was able to differentiate discrete pores. Then the Analyze Particles function that is built into Image J was used to determine the area of each pore and to count the number of pores in within a given area range.

3.3.1. Influence of Sugar Concentration on Porosity and Pore Size Distribution

The addition of sugar to the suspo-emulsion will result in a higher porosity simply because the sugar takes up some volume and then it is dissolved away toward the end of the production process. The addition of sugar to the suspo-emulsion will result in a higher porosity as long as the suspo-emulsion does not phase separate or phase invert. However, as shown in the phase diagram in Figure 9 in Section 2.5, the addition of sugar generally results in reduced likelihood of phase separation until a critically high

concentration of sugar either causes the foam to become weak and crumble (at low concentrations of isopropanol) or causes phase inversion (at high concentrations of isopropanol). A plot of the sugar concentration versus the porosity of the sample is shown in Figure 20. This figure shows that the porosity of the sample is proportional to the sugar concentration, but the relationship is non-linear due to the influence of the isopropanol.

The pore size distribution is also affected by the concentration of sugar in the sample because the smaller, highly interconnected pores appear to form from the dissolution of the sugar. Figure 21 is a histogram of pore sizes of samples with a constant isopropanol concentration of 1.44g/mL and variable sugar concentration from 2.06g/mL to 5.15g/mL in 1.03g/mL increments. This histogram shows that there are more pores in the sample when the sugar concentration is increased. Figure 22 and Figure 23 are plots of the sugar concentration in the suspo-emulsion versus the average pore sizes and standard deviation of the pore sizes, respectively. The average pore size and the standard deviation of the pores sizes are both reduced as the sugar concentration in the suspo-emulsion is increased, showing that the pores are becoming smaller and more uniform in size since the pores generated by the dissolution of the sugar particles are smaller than the pores generated by the expansion of isopropanol.

3.3.2. Influence of Isopropanol Concentration on Porosity and Pore Size Distribution

An increase in the isopropanol concentration will also result in an increased porosity, as shown in Figure 24, which is a plot of the isopropanol concentration versus porosity. The more isopropanol added into the slurry, the more bubbles and pores are created. There is, however, a limit to how much isopropanol can be added to the slurry, as an increase in isopropanol concentration results in an increased likelihood of phase separation as described previously in Section 2.5.

While the smaller and more highly interconnected pores appear to be from the sugar template, the larger pores are from the expansion of isopropanol. The pores from the sugar template are generally open-celled, but the throats (the connection between two pores) appear to be smaller.

Figure 25 is a histogram of pore sizes of samples with constant sugar concentration of 5.15g/mL and variable isopropanol concentration from 1.03g/mL to 1.86g/mL in 0.206g/mL increments. This histogram shows that there are fewer pores in the sample when the isopropanol concentration is increased. Figure 26 and Figure 27 are plots of the isopropanol concentration in the suspo-emulsion versus the average pore size and standard deviation of the pore sizes, respectively. The average pore size and the standard deviation of the pores sizes are both increased as the concentration of isopropanol in the solution is increased indicating that the pores become larger and are more heterogeneous in size.

3.4 Ultimate Tensile Strength

The Ultimate Tensile Strength (UTS) of a material is a measure of the maximum tensile stress that a material can withstand before breaking. The value of the point with the largest tensile stress on a tensile stress-strain curve is the UTS and it is measured in units of force per unit area (Pascals). The UTS is an especially important parameter for foams because foams tend to tear easily compared to their bulk material counterparts. Experimentally, the procedure for measuring both the UTS and the Young's modulus follows the ASTM Standard D3574 for cellular materials. The foam samples are extended at a rate of 500mm/min with measurements of the load and the extension taken every 50 microseconds. The samples are required to have a constant cross sectional area and are extended until they break. The suspo-emulsions are prepared in the same manner

as before and molded into cylinders with a diameter of approximately 0.75 inches. Each sample's diameter was measured to ensure that no errors arose from the assumption that the diameter of each sample was exactly the same, as the cross sectional area is used to calculate the Young's modulus. The samples were tested until failure on an Instron 4400 tensile test machine with a 250N load cell. The data collection program was Bluehill and was set up to take all the data necessary to calculate the UTS and Young's modulus. Three samples for each composition were tested and averaged. An example of a stress-strain diagram generated from the tests is shown in Figure 28.

The results of the tests are shown in Figure 29. In general, the UTS of the foam decreased with an increased sugar concentration. This is due to the decrease in density of the foam that results from overfilling with sugar. This is the usual trend for silicone foams, as a decrease in density normally results in a decrease in the UTS[16].

Conversely, an increase in the isopropanol concentration results in an increase in the UTS of the foam. This is attributed to the hierarchical structure that is formed from the interplay of the isopropanol pores and the pores formed by the dissolution of sugar.

The UTS is plotted against the density of the foam samples in Figure 30. The trials with the same sugar concentration are grouped with ovals around them, and trials with the same isopropanol concentration are grouped by symbol. It is clear that as more isopropanol is added to the suspo-emulsion at a constant sugar concentration, the density of the resulting foam is decreased and UTS values are increased. Sugar appears to have an adverse effect on the UTS of the foam, but that is in part due to the reduction of density of the foam, which is known to decrease the strength of polymer foam[16].

3.5 Young's Modulus

The Young's modulus (or tensile modulus or modulus of elasticity) of a liner elastic

material characterizes the stiffness of the material and is defined as the ratio of tensile stress over tensile strain. For the case of silicone foam, the Young's modulus is determined for small strains where the stress-strain curve is linear. The equation for the Young's modulus is:

$$E = \frac{\sigma}{\varepsilon} \tag{7}$$

Where E is the Young's modulus, σ is the tensile stress, and ε is the tensile strain. When determining the Young's modulus of a material, the tensile stress is simply the force applied to the material divided by the cross sectional area of the material sample, as shown in Equation 8:

$$\sigma = \frac{F}{A_0} \tag{8}$$

Where σ is the tensile stress, F is the force applied to the sample, and A_0 is the initial cross sectional area of the sample. The tensile strain is the change in length of the material sample divided by the initial length of the material sample as displayed in Equation 9:

$$\varepsilon = \frac{\Delta L}{L_0} \tag{9}$$

Where ε is the tensile strain of the material, ΔL is the change in length of material sample from its initial length to its final length, and L_0 is the initial length of the material sample.

Figure 31 shows the isopropanol concentration versus the Young's modulus of the resulting foam. Interestingly, at a sugar concentration of 2.06g/mL, the isopropanol concentration has a drastic increasing effect on the Young's modulus of the foam. There also appears to be very little difference between the moduli of foams that were made with

a sugar concentration of 3.09g/mL and 4.12g/mL, while foams made with a sugar concentration of 5.15g/mL show a significant decrease in moduli values.

Figure 32 is a plot of the density versus the Young's modulus with the samples grouped by sugar content in ovals, and grouped by isopropanol content by symbol. From this graph it can be seen that an increase in sugar concentration reduces the density of the foam, but also significantly reduces the Young's modulus. It is also evident that an increase in isopropanol concentration reduces the density and increases the Young's modulus. This pattern appears to hold true for all sugar concentrations. Therefore, to obtain the highest Young's modulus with the lowest density, one would want to have as much isopropanol as possible with as little sugar as possible (while avoiding phase separation and phase inversion!).

Chapter 4

Application to Maritime Oil Spills

4.1 Introduction

The foam produced from this process has the potential for use in the cleanup of oil spills that occur in bodies of water because of its oleophilic and hydrophobic nature. Oil spills have a tremendous negative environmental and economic impact [61, 62] and are extremely costly and time consuming to clean up. Environmental repercussions of oil spills include the loss of animal life and habitats, and the introduction of harmful chemicals into their food supply [63-68]. Aside from the obvious economic effects of reduced profits to oil companies and increased gasoline prices [69], oil spills can destroy the main source of income for fishing communities and create economic downturns in travel destinations [70]. In the case of the British Petroleum Gulf of Mexico oil spill in 2010 over $20 billion has been set aside for litigation and environmental remediation costs [71].

Due to the obvious importance of oil spill cleanups, several methods of removing oil from water have been developed. There exist large and expensive equipment that use oleophilic/hydrophobic spinning disks to selectively adsorb oil to their surface as a protrusion scrapes the oil off. However, these machines are only effective close to the site of the spill where the concentration of oil is high [72, 73]. A centrifuge that spins a mixture of oil and water can also be used to separate oil from water based on their different densities, as the oil will remain in the center of the centrifuge while the water is pushed to the edges [72]. These machines can process large volumes of contaminated water; however the concentration of oil in the processed water would still be above the environmentally safe level of 10ppm [68, 74]. Skimmers, as their name implies, attempt to skim the oil slick off of the surface of the water, although they require calm water to be effective [75]. These methods are used where there is a high concentration of oil, usually

near the site of the spill, but are not effective as the oil slick spreads far away [76-78]. Dispersants are used to break up an oil slick into oil droplets that can be diluted into the volume of the water rather than lie at the surface. Dispersants themselves tend to be toxic, especially in conjunction with oil [68, 79].

Further away from the site of the spill, absorbent materials can be used as they can more selectively absorb oil that exists in lower concentrations [80]. Though oil and water are immiscible, most porous, spongy materials will readily absorb both oil and water [81, 82]. This is unfavorable because the oil tends to create a thin film on the surface of the water that is easily emulsified (albeit unstably), creating a situation where water is just as likely to be absorbed as the oil. This makes non-selective absorbent materials not economical for oil cleanup. Our silicone selectively absorbs oil instead of water and the absorbed oil can be removed by compressing the foam.

4.2 Oil Absorption Test

The lower the density of an open-cell foam, the more oil it should be able to absorb due to the increased void space, however, some of the pores may be closed - leading to less oil absorption capacity. Thus, an oil absorption test where the mass of the sample is measured before and after being placed on a simulated oil slick was developed to allow for a more direct measurement of the performance of the different foam compositions. Cylindrical samples measuring 0.75 inches in diameter were placed atop a Petri dish that was filled with ExxonMobil 5W-30 motor oil. The cross sectional area of each of the sample was held constant so that a before test mass and after test mass could be easily compared between the samples. Since PDMS is oleophilic, the motor oil was readily absorbed. After 1 minute the sample was removed and the mass was recorded again. This was also repeated for time period of 15 seconds instead of 1 minute to determine the

effect of time on the absorption performance. As a performance measure, the weight gain of the foam was calculated using the following equation:

$$MG = \frac{M_f - M_i}{M_i} \quad (10)$$

Where, MG is the mass gain, M_f is the final mass of the sample and M_i is the initial mass of the sample. Figures 33 and 34 are plots of the normalized mass gain vs. isopropanol concentration in the suspo-emulsion for 1 minute and for 15 second tests, respectively. Each test shows that an increase in isopropanol slightly increases the normalized mass gain of oil, and an increase in the sugar concentration more drastically increases the normalized mass gain. The difference between the two tests shows that the majority of the oil absorption occurs within the first 15 seconds of the test, because the values for the 15 second test are greater than half of the values for the 1 minute test. This would be expected because over time there will be less void space for the oil to fill in as the oil is being absorbed. Figures 35 and 36 are plots of the density of the foam versus the normalized weight gain for the 1 minute and 15 second tests, respectively, and it is easy to verify that lower density foams show higher normalized weight gains in both instances. It is also obvious that all the foams show higher weight gains in the 1 minute test compared to the 15 second test. It is apparent from this test that the sample made with the largest concentrations of isopropanol and sugar performed the best, specifically; the sample made with 1.86g/mL of isopropanol and 5.15g/mL of sugar performed the best.

Chapter 5

Conclusion and Outlook

5.1 Conclusion

A process to create hierarchical open cell silicone foams from a blowing agent slurry/liquid polymer suspo-emulsion was developed. The processing parameters to obtain open cell foams, closed cell foams, particles (phase inversion) and phase separation were elucidated. Sugar in the suspo-emulsion was found to have a stabilizing effect on the suspo-emulsion due to a thickening effect, while isopropanol had a thinning and destabilizing effect. Bubbles generated during the foaming process and FE-SEM micrographs were analyzed to expose the physical foaming mechanism. The parameter window for open cell foams was then studied in detail by studying morphological, mechanical and physical properties. Morphology of the foam samples tended to be hierarchical with most pores ranging from tens of microns to hundreds of microns in diameter. Curing temperature and concentrations of isopropanol and sugar affected pore morphology in a predictable manner. We found that the Ultimate Tensile Strength and Young's Modulus of the foam was highly dependent on the density of the foam, but improved mechanical properties and lower density could be obtained by increasing the concentration of isopropanol in the suspo-emulsion while staying within the processing window. These open cell foams were then tested for their oil absorption performance and it was found that the best performing foam was made from the suspo-emulsion with the highest concentrations of sugar and isopropanol tested (5.15g/mL and 1.86g/mL, respectively).

5.2 Outlook

Future work on this method of foaming polymers can be broken down into several areas: different input materials, suspo-emulsion phase diagrams, applications and large

scale manufacturing.

As is usual with any foaming process that uses a liquid blowing agent, there is generally a tradeoff between the boiling point of the blowing agent and its environmental friendliness. Water has a relatively high boiling point so its use as a blowing agent is rather limited. Nonetheless, I believe it is the logical next blowing agent that should be explored for this process. A solar oven may be the environmentally friendly way to overcome the larger energy requirement for vaporization. Since sugar is more soluble in water than it is in isopropanol, the process will likely require a higher sugar concentration to achieve the necessary viscosity to prevent phase separation.

The phase diagram for the suspo-emulsion may very well raise the most scientifically interesting questions. There appear to be at least five regions for end products as shown in Figure 6, and they appear to be well defined. But what determines the equations of the lines that separate the regions? Phase separation can be induced by heat, so phase diagrams at different temperatures should be performed. By creating phase diagrams for several material systems at different temperatures, we may be able to find general equations for each of the regions based on material properties (and curing temperature) and thus be able to predict the outcome for new material systems/temperatures. Does the size of the porogen particles affect the stability of the suspo-emulsion? Or whether or not the foam will crumble? Nanocrystalline sugar could create drastically different suspo-emulsions and foams. Could we push the phase separation boundary beyond its natural limit by adding a surfactant? Even for the current PDMS/isopropanol/sugar suspo-emulsion the PDMS particles that are created at high sugar and high isopropanol concentrations are a mystery. Can their size and shape be controlled? They do not appear to be perfectly spherical. Are sugar particles embedded

inside the PDMS particles? On their surface? Can the sugar particles be extracted if they happen to be embedded?

Another area that needs to be tackled is the scalability of the process for the open-cell foam. The three areas of concern are high shear mixing of the components to create the suspo-emulsion, evaporation of the blowing agent and dissolution of the sugar from the final structure. High shear mixing is accomplished with a centrifugal mixer in the lab, but a rotary immersion mixer is likely necessary for manufacturing, so the phase diagram may be affected by a different mixing mechanism. Evaporation of the blowing agent could be hazardous at a large scale because of the flammability of isopropanol vapor, so it will likely have to be sequestered during production. Depending on the final geometry and size of the foam, dissolving the porogen may take a significant length of time. Thin foam sheets are ideal because of their high surface area to volume ratio, but actively driving water through the foam should also reduce the time for dissolution.

In addition to petroleum oil absorption, applications for the open-cell foam region of the PDMS/sugar/isopropanol phase diagram are lipid separation and bioscaffolds. Cooking oils need to be separated from watery organic plant matter, as do lipids from many dairy products, so there may be a process that this foam is well suited to. Since PDMS is chemically inert after it has been crosslinked, it is also biocompatible. Living cells have been shown to react to the structure of the scaffold that they are placed on, so control over the pore morphology of the scaffold is important, and this technique could create large pores for living cells to attach to while leaving smaller pores open to transport nutrients. This process may also be used with biopolymers to create a bioscaffold that dissolves in the body.

Figures

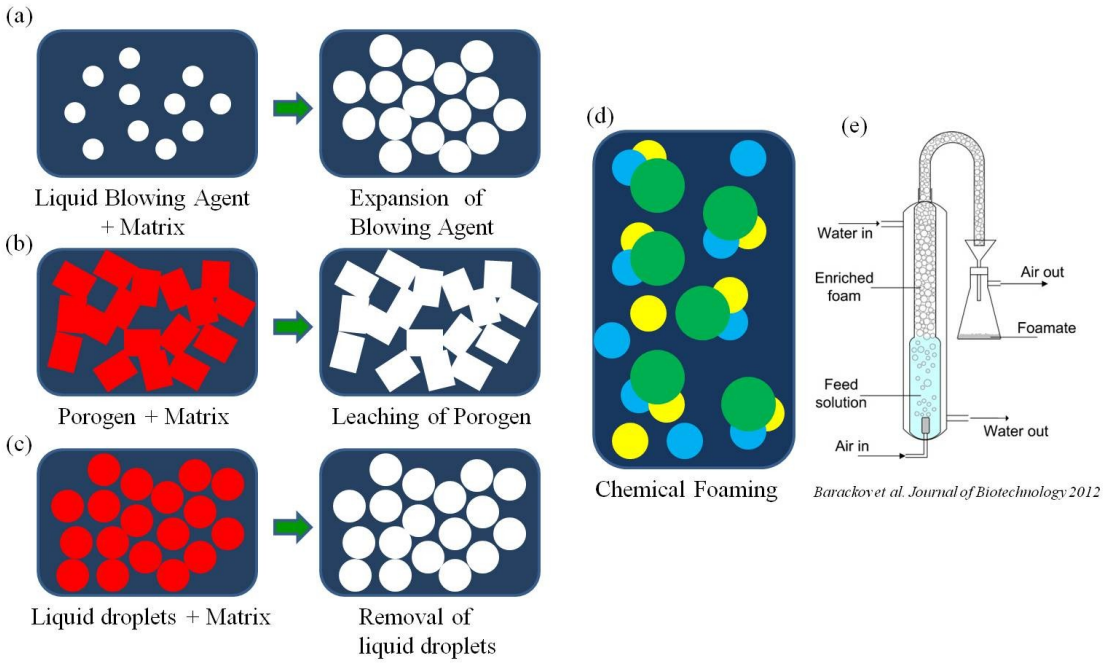

Figure 1. Schematics for the basic polymer foaming mechanisms. (a) Liquid blowing agents are mixed into a liquid polymer and expanded during heating. (b) Porogens (solid particle pore generators) are embedded in a liquid polymer matrix and then removed after solidification. (c) An immiscible liquid is emulsified with a liquid polymer and then the droplets are removed. (d) Gaseous blowing agents can be created from a chemical reaction within the polymer or (e) physically blown into a liquid

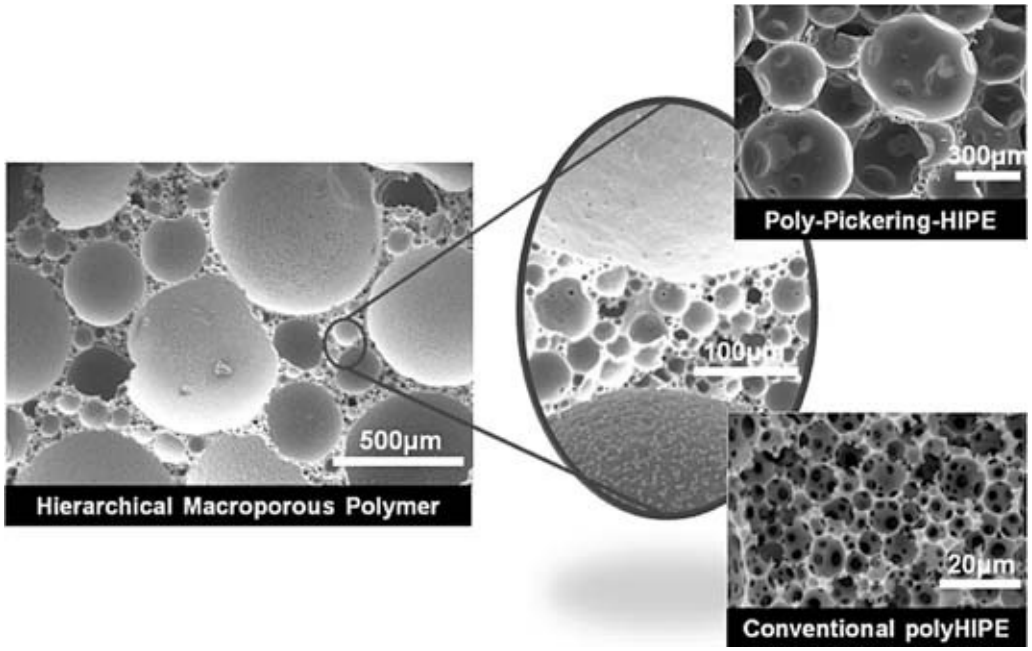

Figure 2. Hierarchical macroporous polymer foam created from an emulsion stabilized by both particles and surfactants at the droplet interface. Large pores created from the particle stabilized droplets are surrounded by smaller pores created from the surfactant stabilized droplets [17].

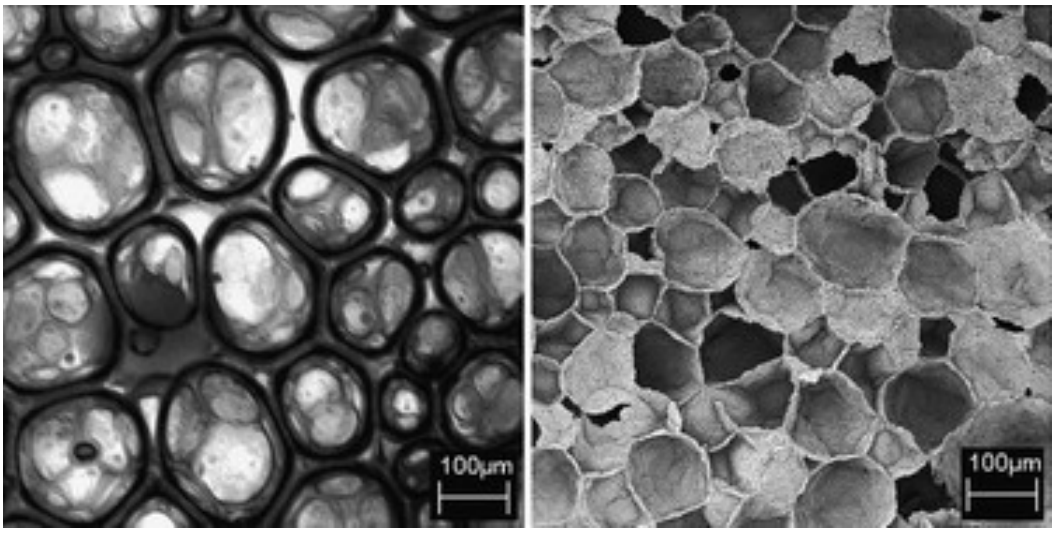

Figure 3. An aqueous foam stabilized solely by thermoplastic polymer particles (left) is heated until the water evaporates and the polymer particles are sintered together into a solid structure (right) [49].

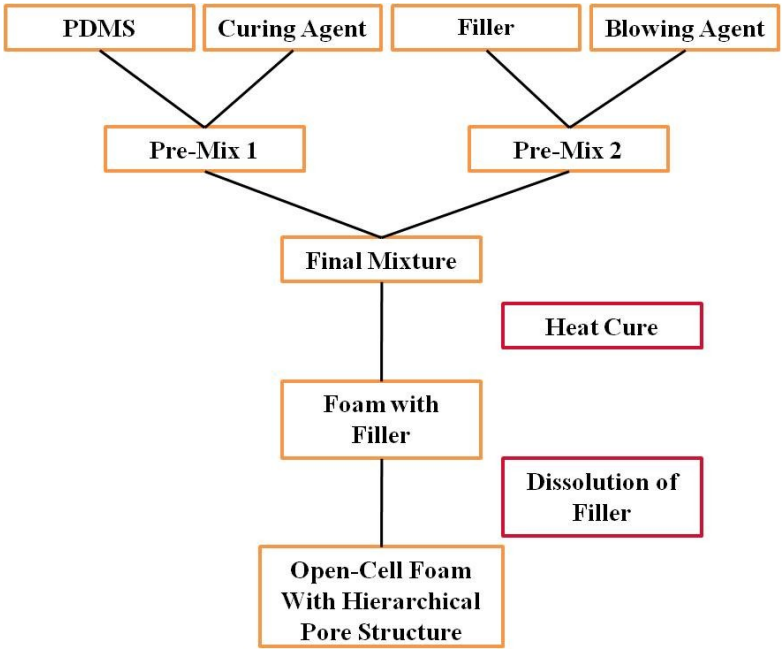

Figure 4. A flow diagram representing the production process of open-cell hierarchical foams.

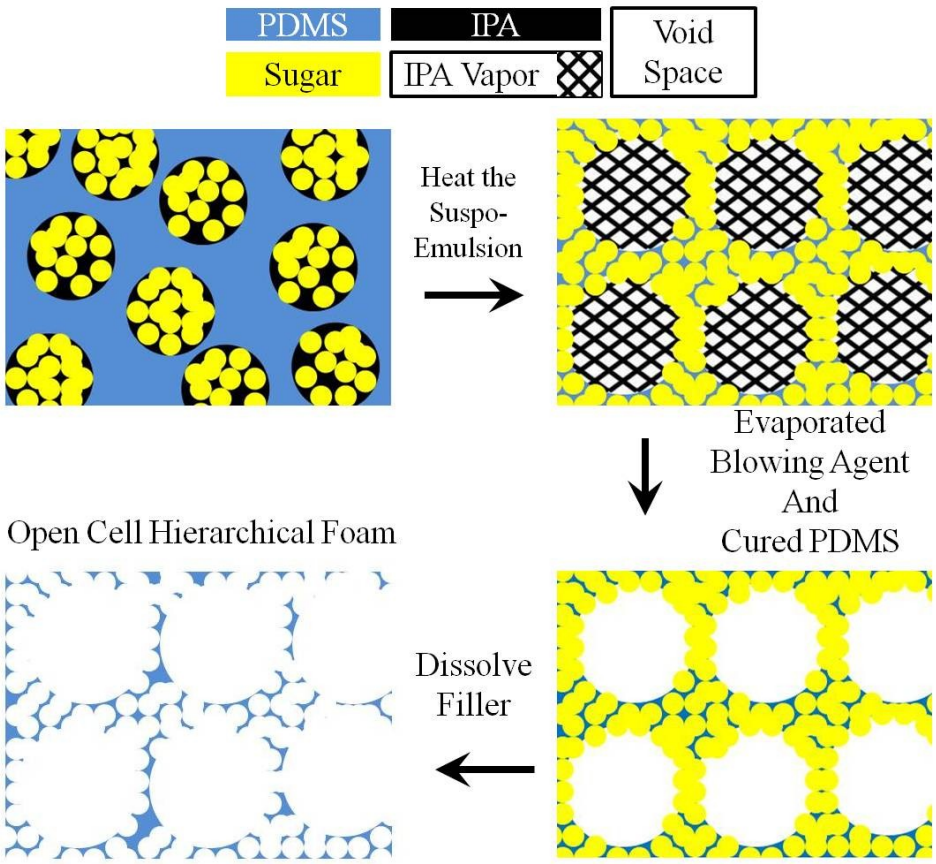

Figure 5. A schematic of the process after the suspo-emulsion has been made. Heating vaporizes the isopropanol and eventually causes it to evaporate, but not before the PDMS has cured. When the sugar is dissolved, voids are left in the PDMS structure.

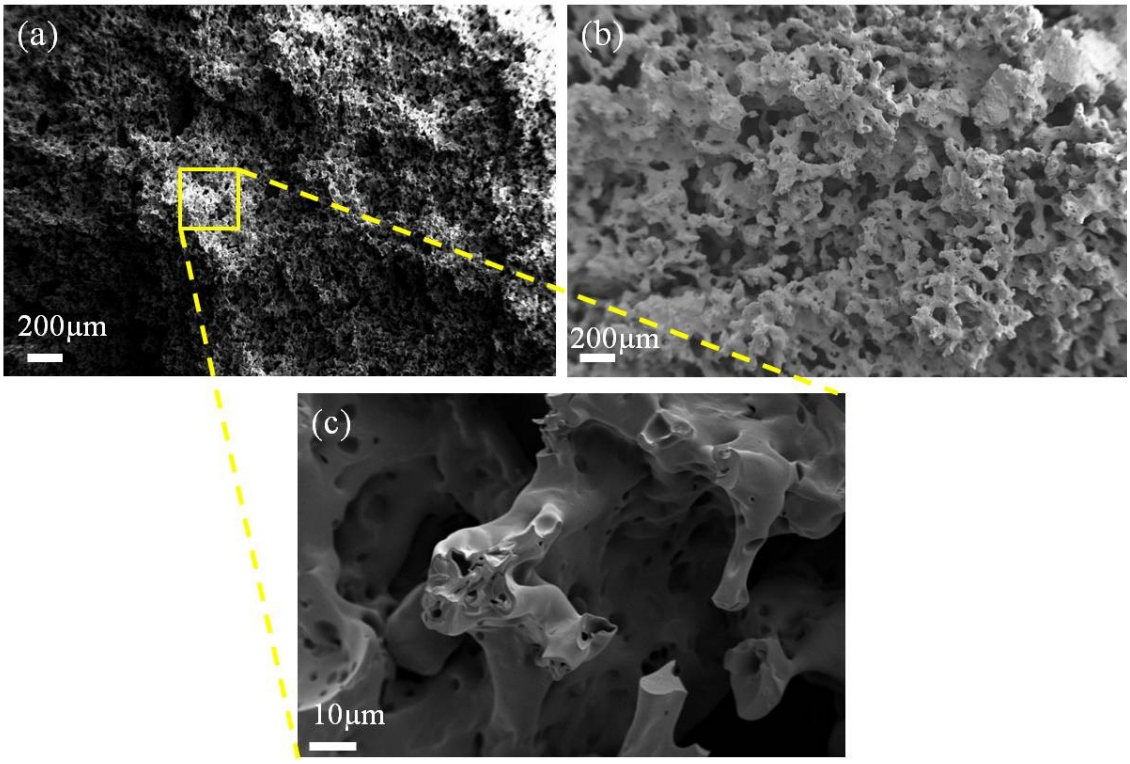

Figure 6. FE-SEM micrographs of the resulting foam using the proposed process. Epoxy resin was used instead of PDMS to demonstrate the versatility of the process. (a) is a micrograph of the foam that results from carrying out the process at 25°C, (b) is the foam from the process being carried out at 60°C, and (c) is a close up showing small divots on the cell walls.

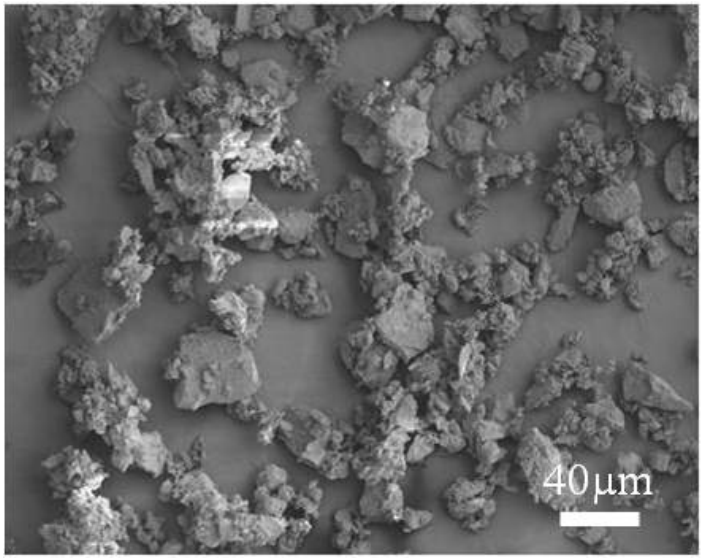

Figure 7. FE-SEM image of the Domino 10X Confectioner's sugar that was used as a dissolvable filler (porogen) in the proposed foaming process.

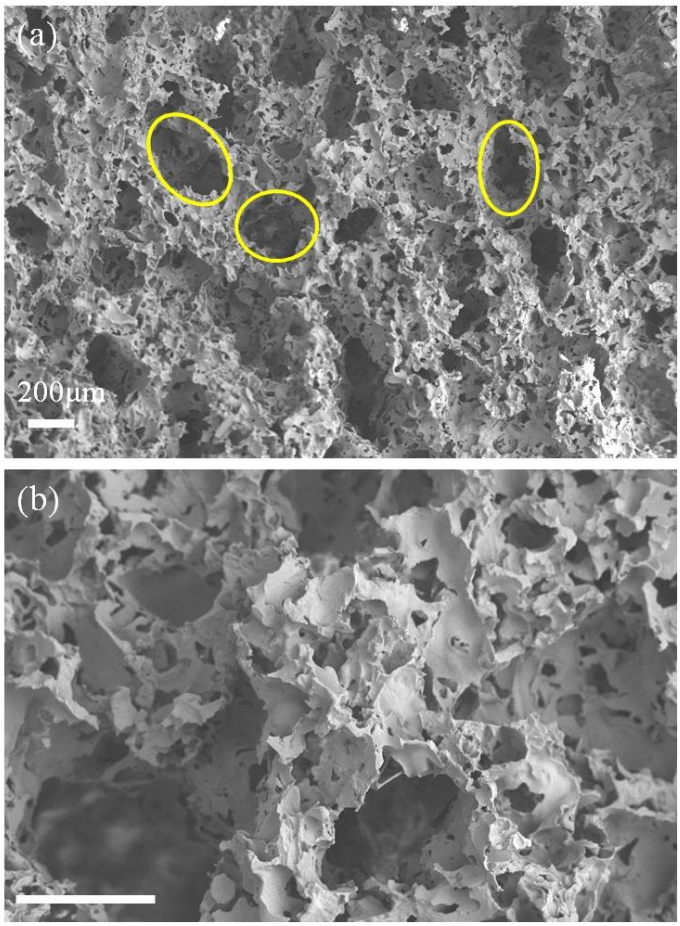

Figure 8. FE-SEM micrographs of the process carried out with sodium bicarbonate ($NaHCO_3$) as the filler instead of powdered sugar. The hierarchical structure is clearly visible in (a), with the large oval pores (three of which are outlined) caused by isopropanol bubbles and the small angular pores formed from dissolving the sodium bicarbonate. (b) is a close up of (a) to give a better view of the pores that are formed from dissolving sodium bicarbonate. All scale bars are 200µm.

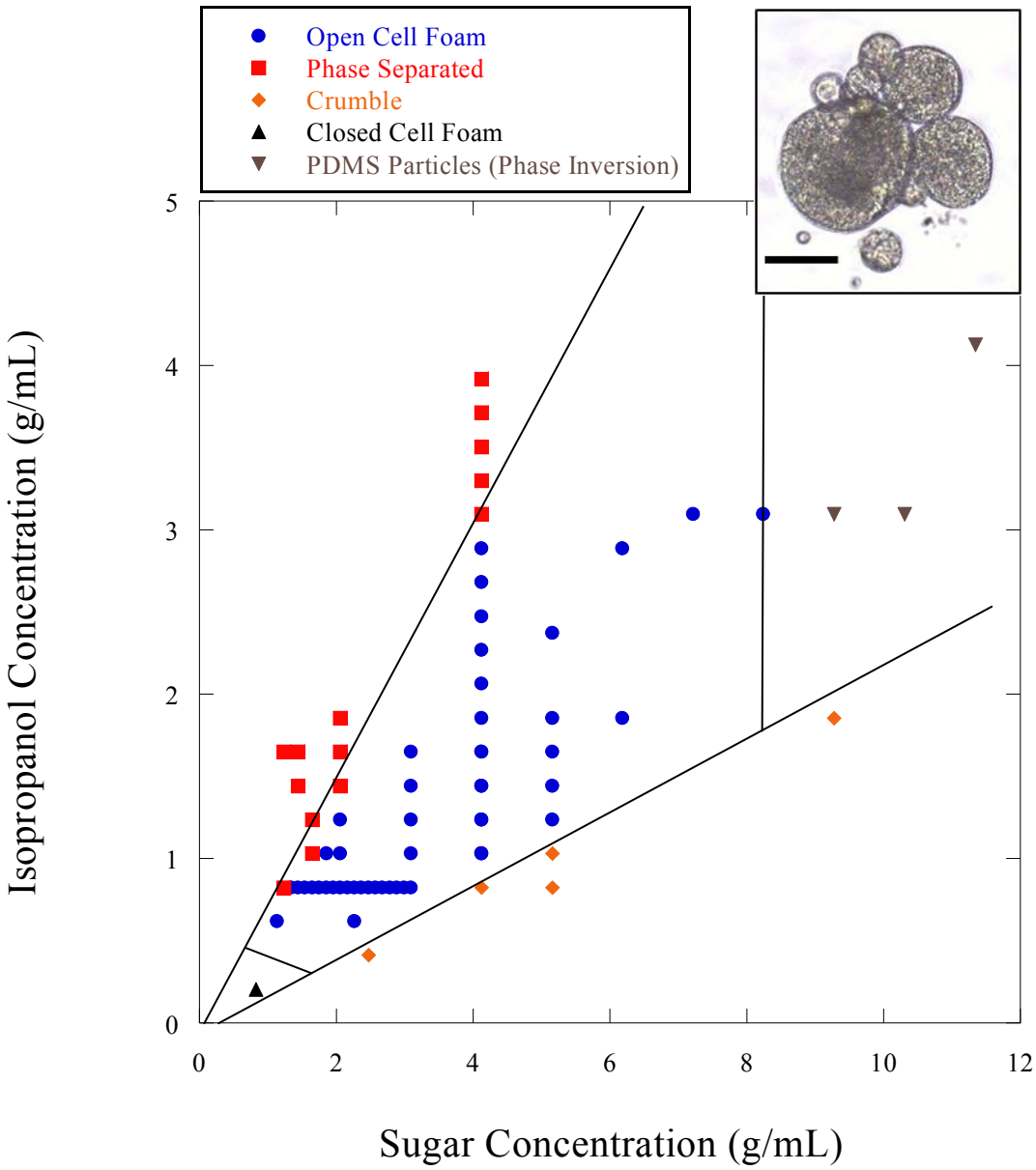

Figure 9. The phase diagram for the production process with the volume of PDMS held constant at 4.85mL and the curing temperature held constant at 80°C. There are five distinct end products depending on the concentrations of isopropanol and sugar. The end product of interest in the systematic study is the open-cell foam. The inset image is a micrograph of PDMS particles (scale bar 300µm) generated from the phase inverted section of the phase diagram.

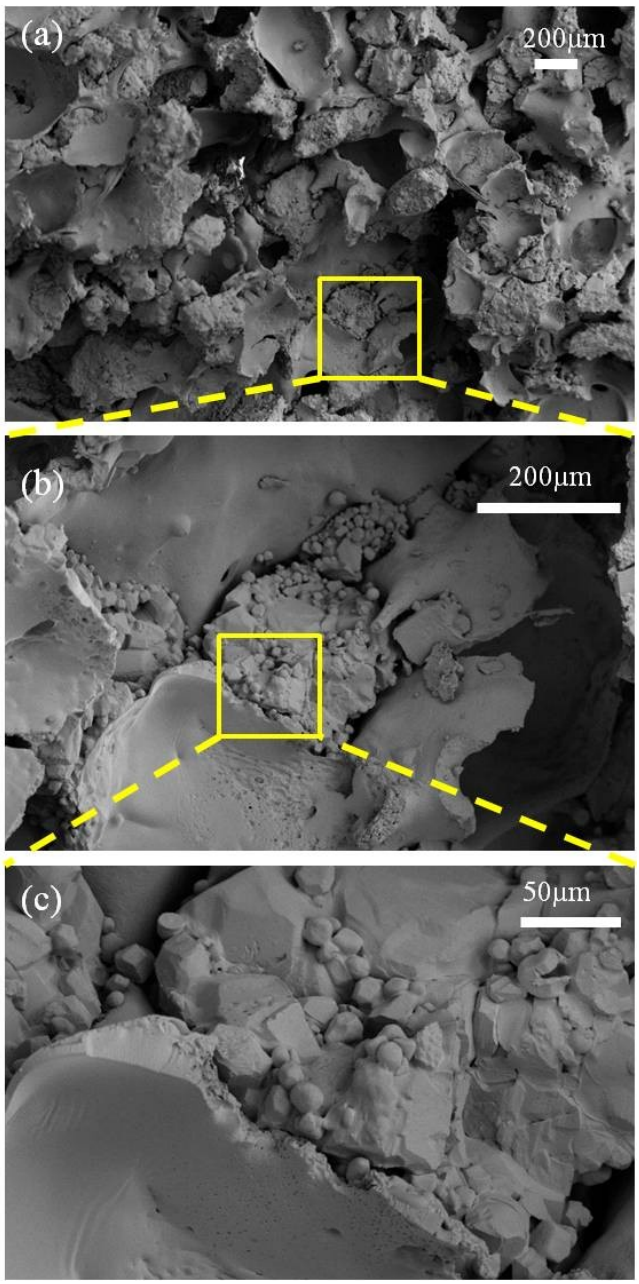

Figure 10. FE-SEM micrographs of a sample of foam before the sugar is dissolved. It is clear that the sugar is pushed together by the expanding isopropanol bubbles and that the sugar lies between films of PDMS.

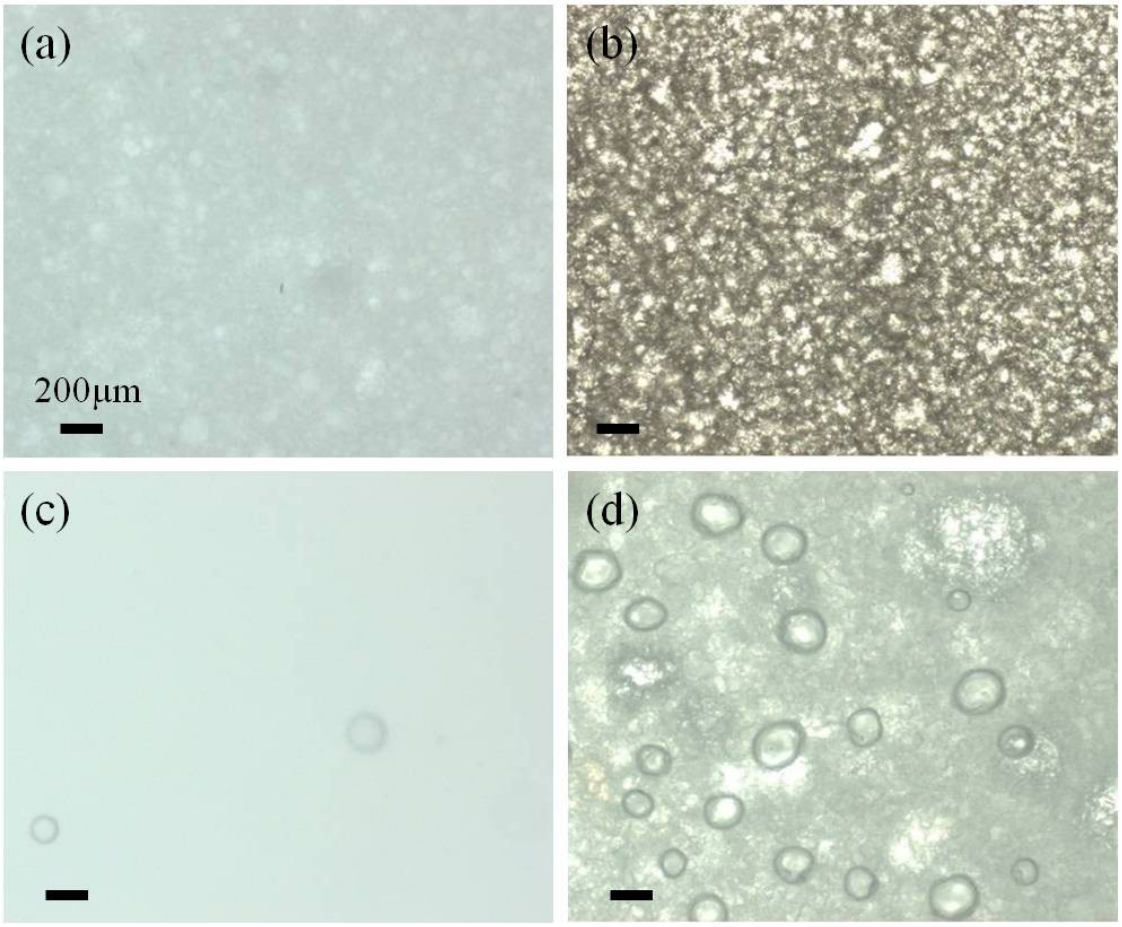

Figure 11. Selected time laps images of thin films made from mixtures of only two of the three required components: (a) PDMS/Sugar, (b) Sugar/Isopropanol, (c) Isopropanol/PDMS. Image (d) represents the sample where all three required components (PDMS/Isopropanol/Sugar) are present. All scale bars are 200 microns.

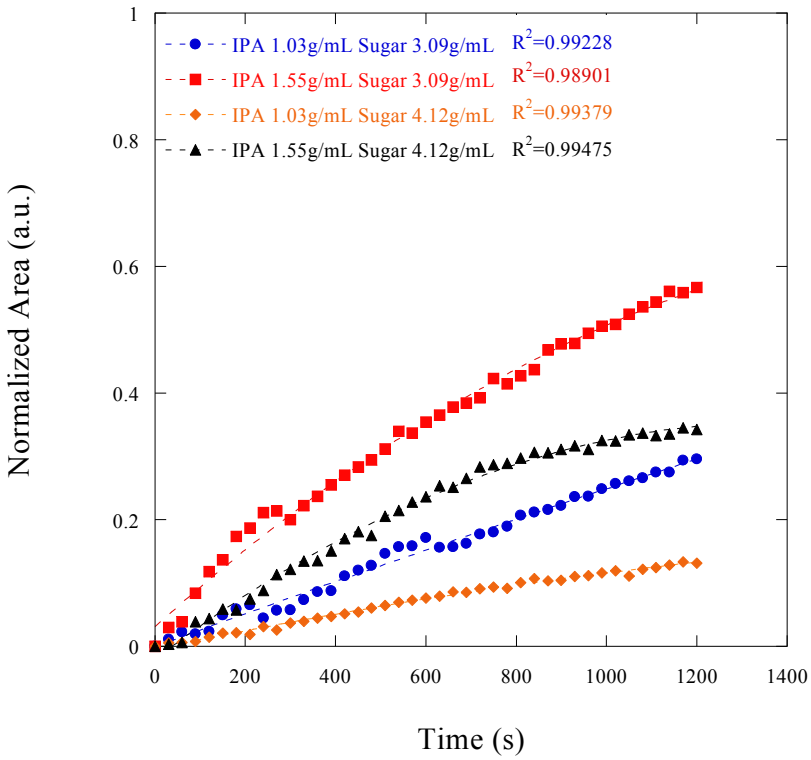

Figure 12. Normalized bubble growth of 1mm thick films of the suspo-emulsion at 25°C. Increasing isopropanol or reducing sugar concentration leads to faster bubble growth. The data is fitted to quadratic curves with the displayed R^2 values.

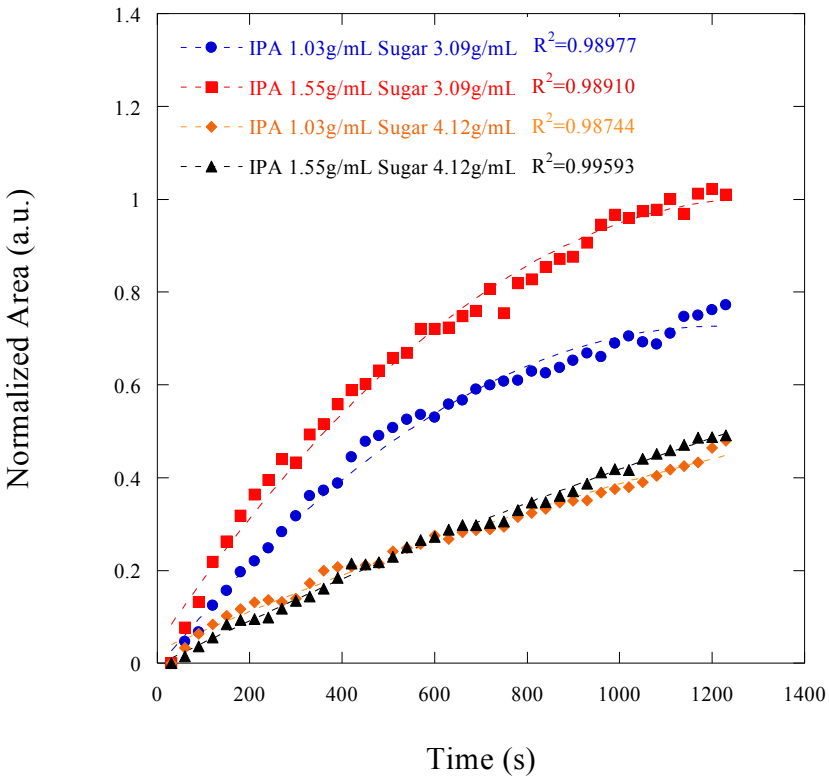

Figure 13. Normalized bubble growth of 1mm thick films of the suspo-emulsion at 38°C. A larger concentration of sugar has a more dramatic negative effect on the bubble size at an elevated temperature. The data is fitted to quadratic curves with the displayed R^2 values.

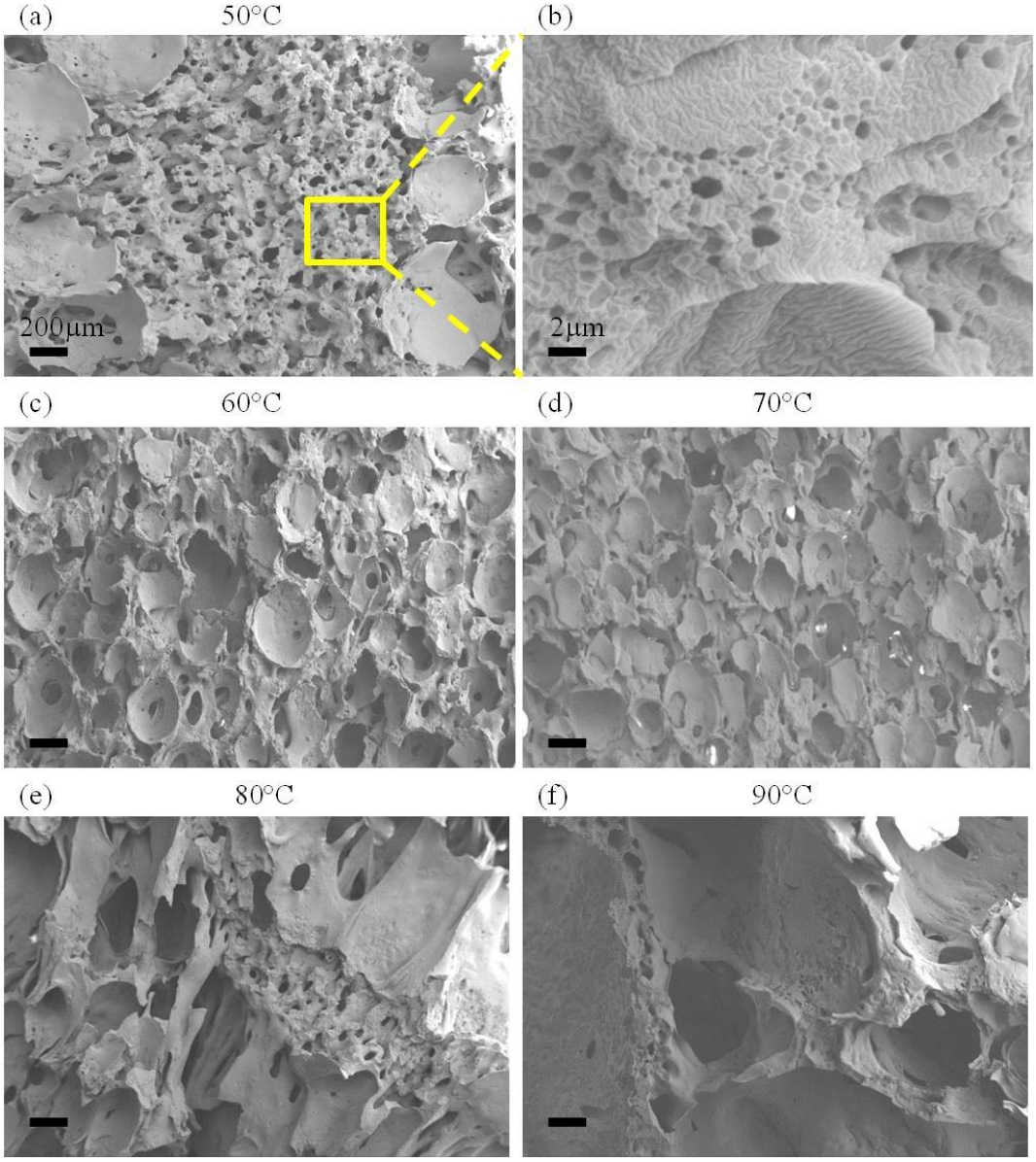

Figure 14. FE-SEM micrographs of the cross section of foams prepared using a composition of 1.86g/mL isopropanol, 4.12g/mL sugar and 4.85mL PDMS at different curing temperatures. (b) is an example of mesoscale pores that can be found in these foams. All scale bars are 200 microns, except for (b) which has a scale bar that is 2 microns.

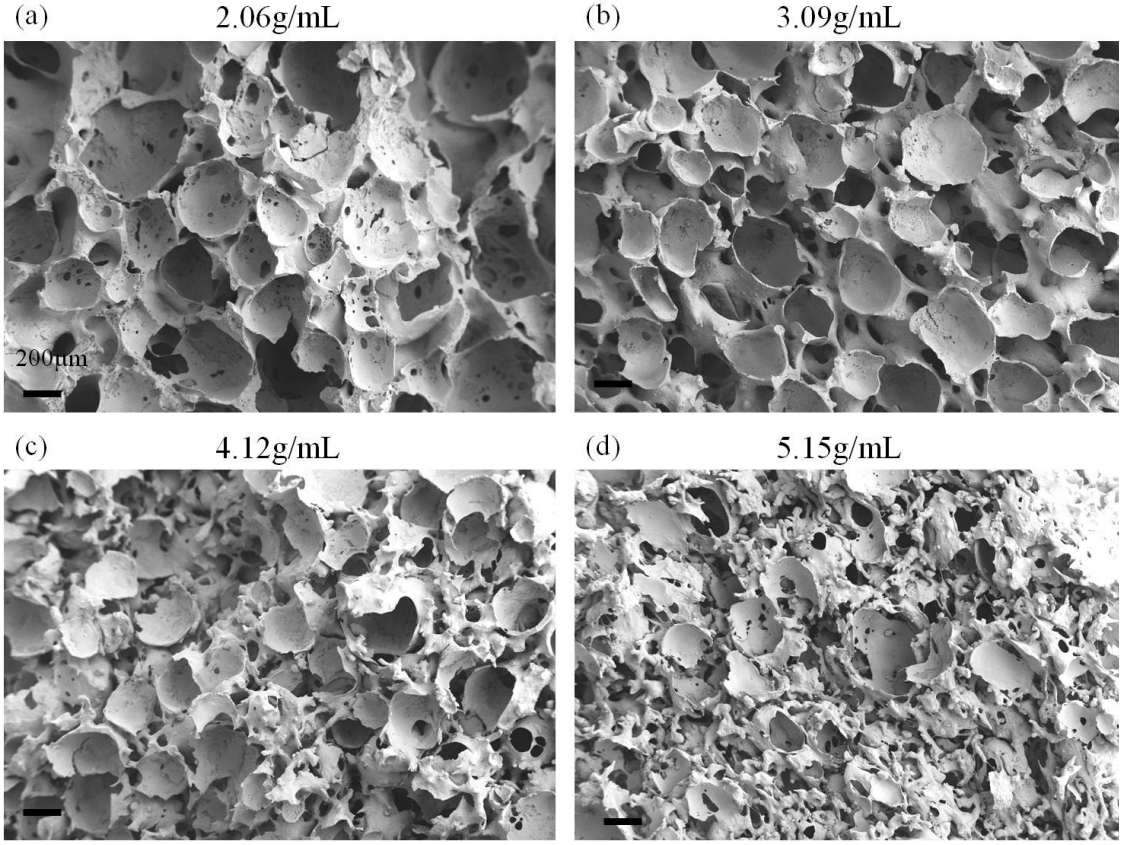

Figure 15. FE-SEM micrographs of foams that all have 1.44g/mL of isopropanol and 4.85mL of PDMS, with various sugar concentrations. As the sugar concentration is increased, the foam morphology becomes dominated by pores resulting from the dissolution of sugar. All scale bars are 200 microns.

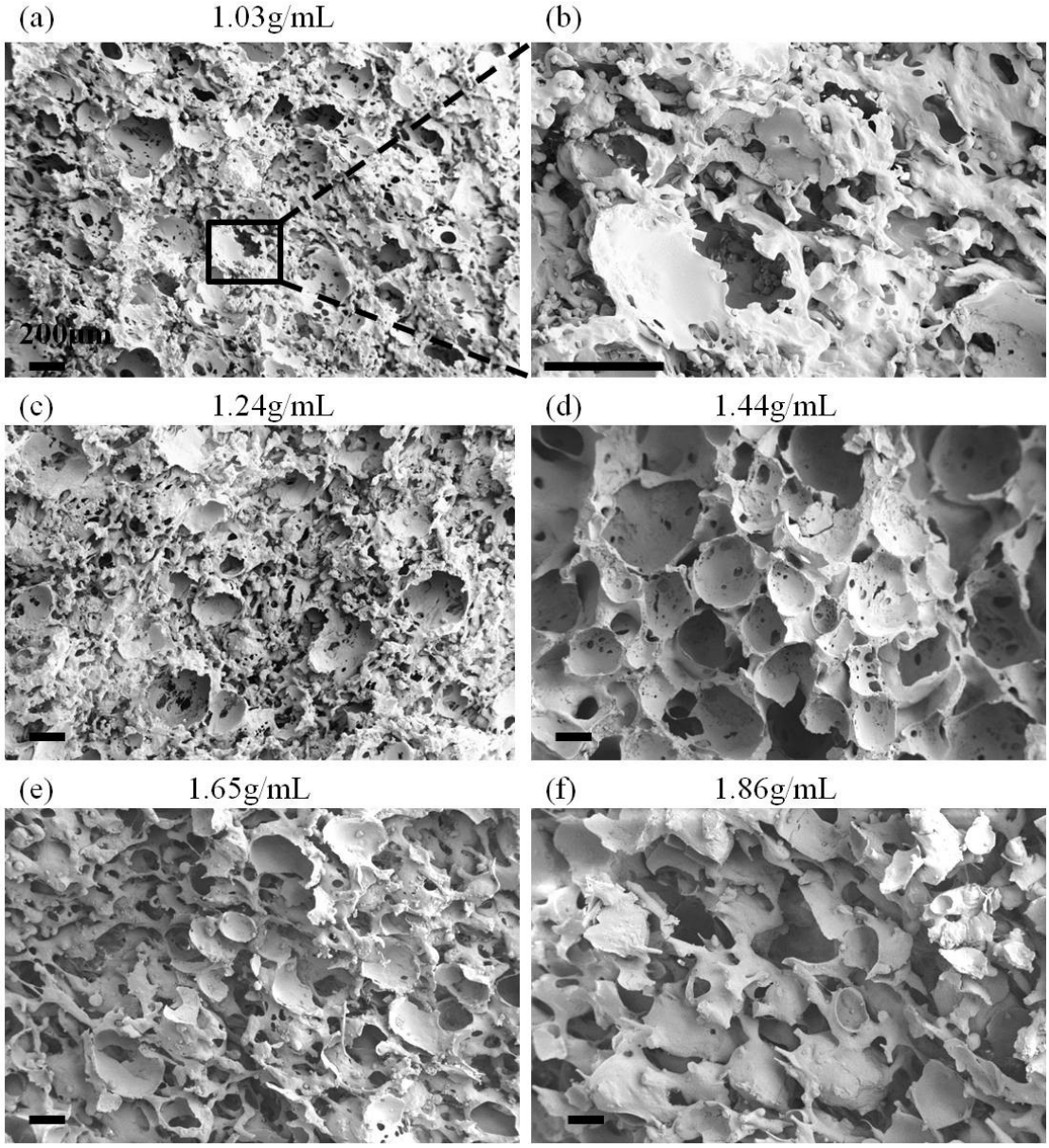

Figure 16. FE-SEM micrographs of foams that all have 5.15g/mL of sugar and 4.85mL of PDMS with different isopropanol concentrations. As the isopropanol concentration is increased the foam morphology becomes dominated by large pores formed by isopropanol bubbles. All scale bars are 200 microns. (b) is a close up of the structure shown in (a).

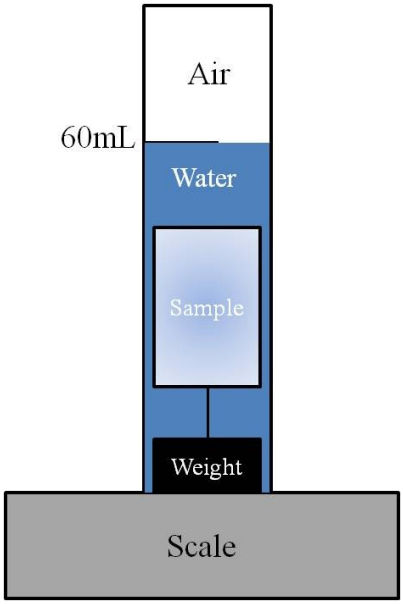

Figure 17. Schematic of the setup for determining the density of the foam samples. An anchor weight of known volume was attached to the foam sample and then placed in a graduated cylinder. The cylinder was then filled with water to a predetermined graduation. The difference between the weight of water and the graduation is the volume occupied by the foam sample and the anchor weight.

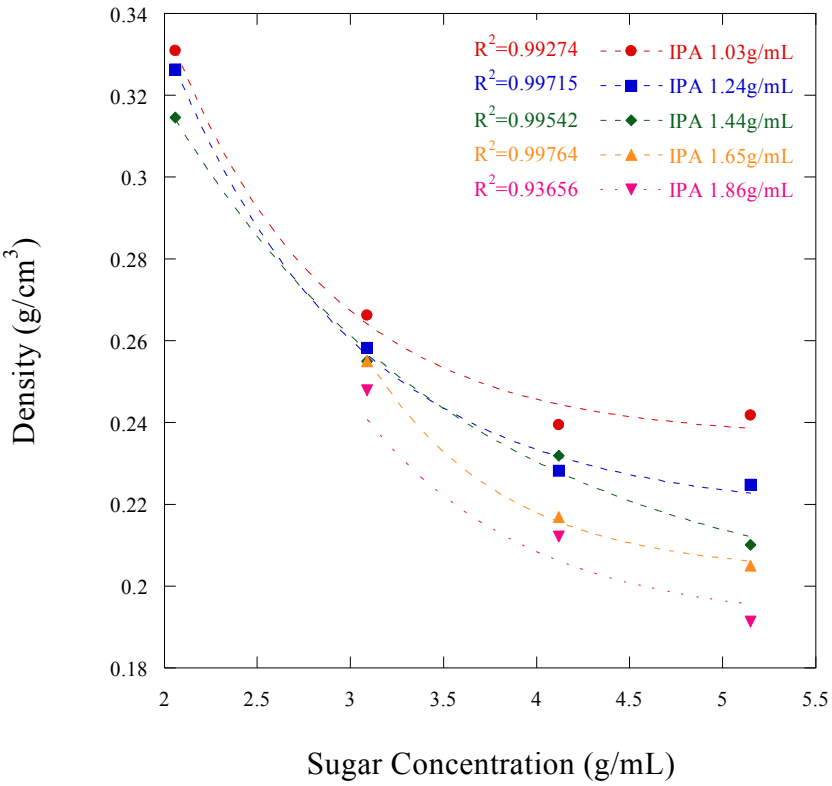

Figure 18. A plot of the density of the foams as a function of the sugar concentration. Changing the isopropanol concentration in the suspo-emulsion has a more drastic effect on the density at higher sugar concentrations, showing that the density is an interdependent function of sugar and isopropanol. The data is fitted to exponential decay functions with the displayed R^2 values.

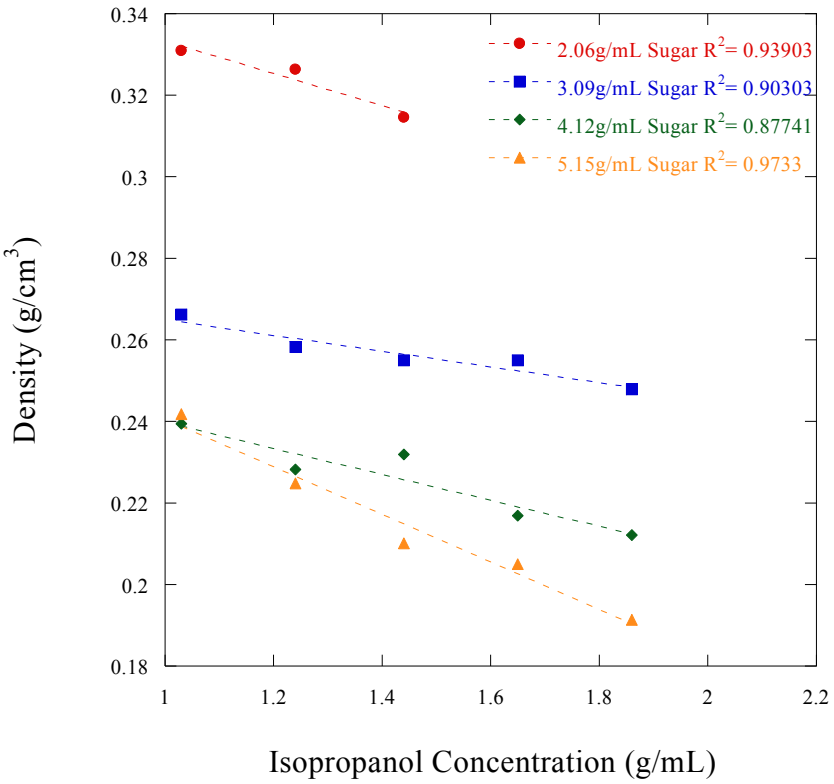

Figure 19. The effect of isopropanol concentration on foam density. The density is inversely proportional to the isopropanol concentration for a given sugar concentration. The data is fitted to lines with the displayed R^2 values.

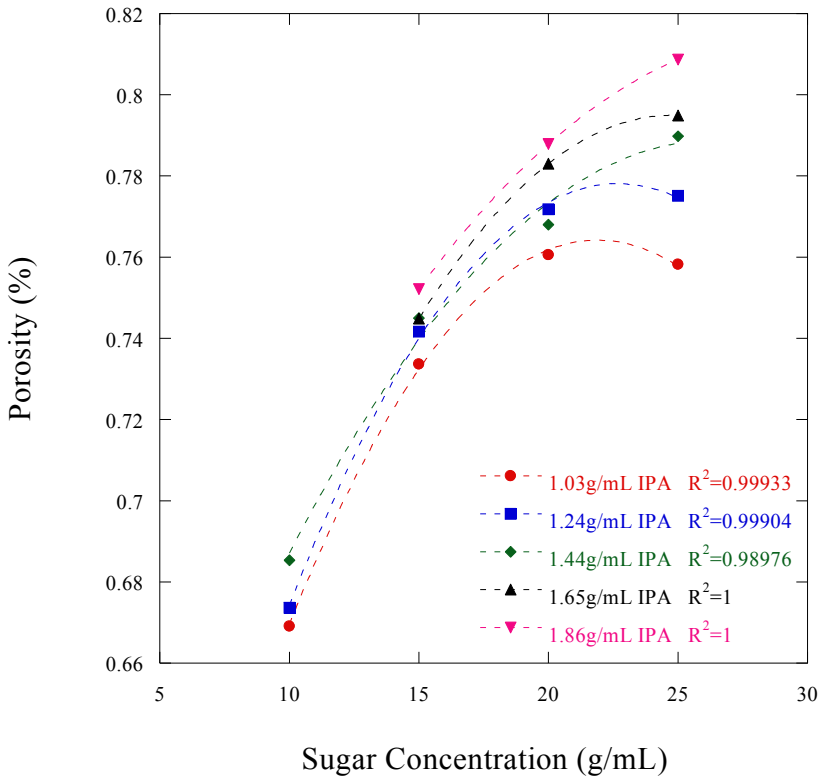

Figure 20. The influence of sugar concentration on the porosity (calculated from the density) of the produced foams. The porosity is proportional to the sugar concentration but at higher sugar concentrations the isopropanol concentration creates greater variation. The data is fitted to quadratic curves with the displayed R^2 values.

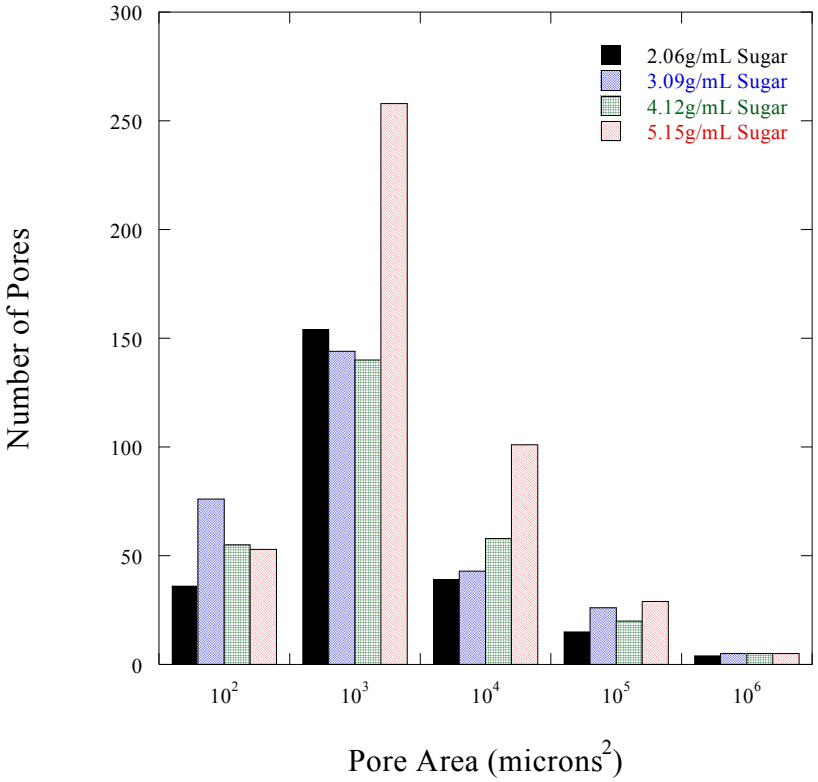

Figure 21. Pore size distribution generated from SEM micrographs for foam samples fabricated with a constant isopropanol concentration of 1.44g/mL. There is a wide distribution of pore sizes and the highest sugar concentration has the greatest number of pores in each bin except for the 10^2 bin.

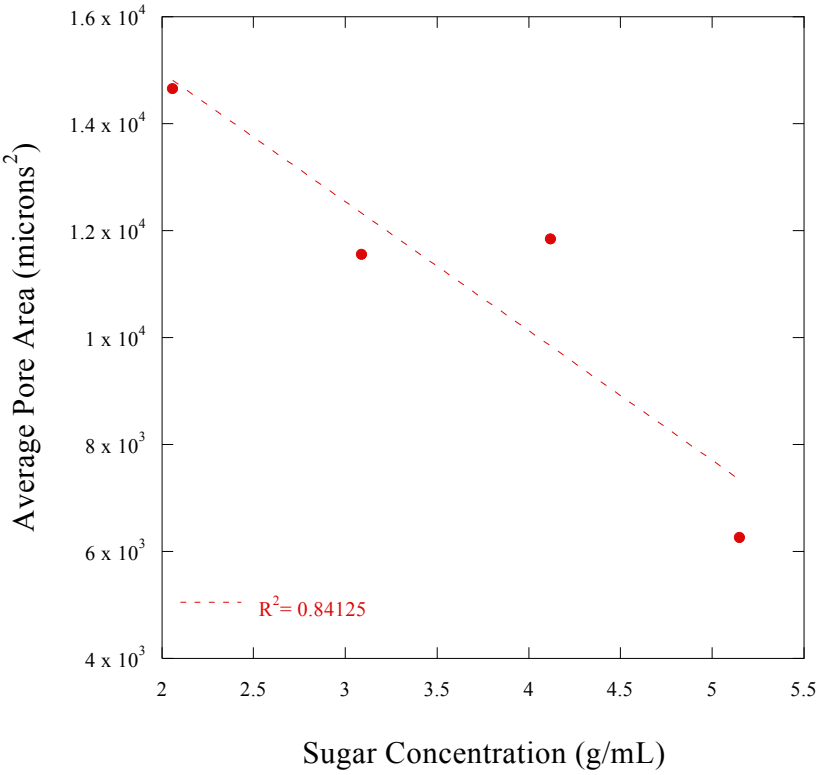

Figure 22. Average pore area generated from SEM micrographs of foam samples fabricated with a constant isopropanol concentration of 1.44g/mL. The average pore area decreases with an increase in the sugar concentration. The data is fitted to a line with an R^2 value of 0.84125.

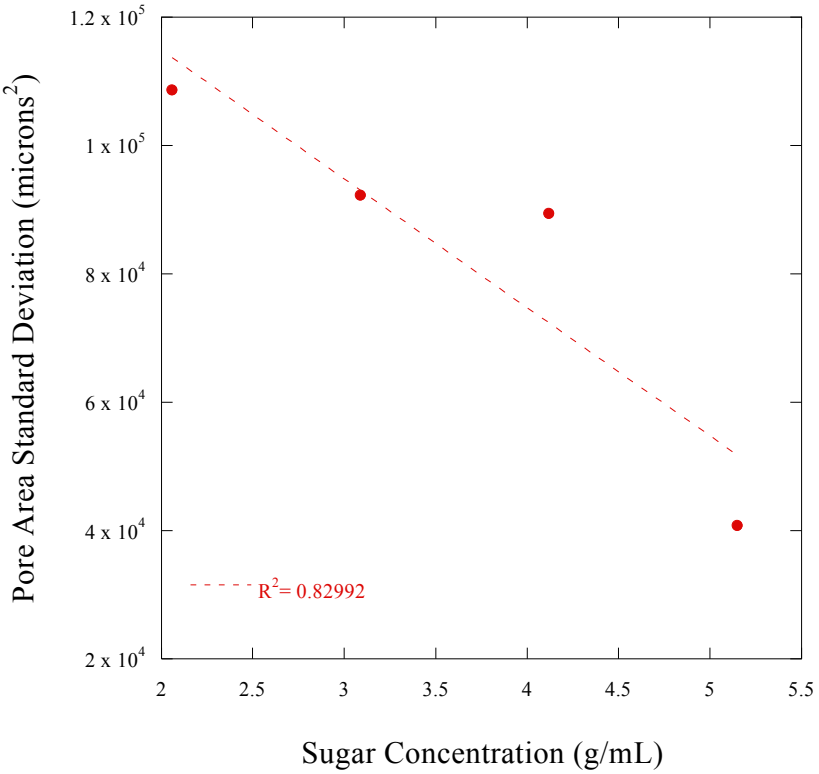

Figure 23. Pore area standard deviation generated from SEM micrographs of foam samples fabricated with a constant isopropanol concentration of 1.44g/mL. The standard deviation of the pore area decreases with an increase in the sugar concentration, indicating that the pores become more uniform in size. The data is fitted to a line with an R^2 value of 0.82992.

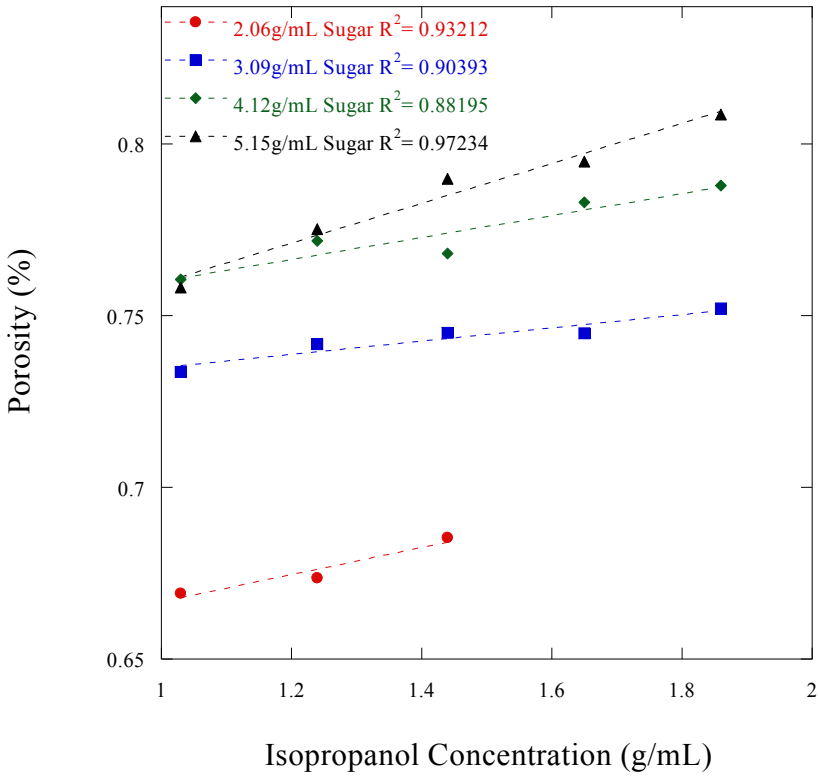

Figure 24. Porosity of foam samples calculated from their densities**.** The porosity of the foam sample is proportional to the isopropanol concentration. There is a comparatively large jump in porosity between the samples prepared with sugar concentration of 2.06g/mL and 3.09g/mL. The data is fitted to lines with the displayed R^2 values.

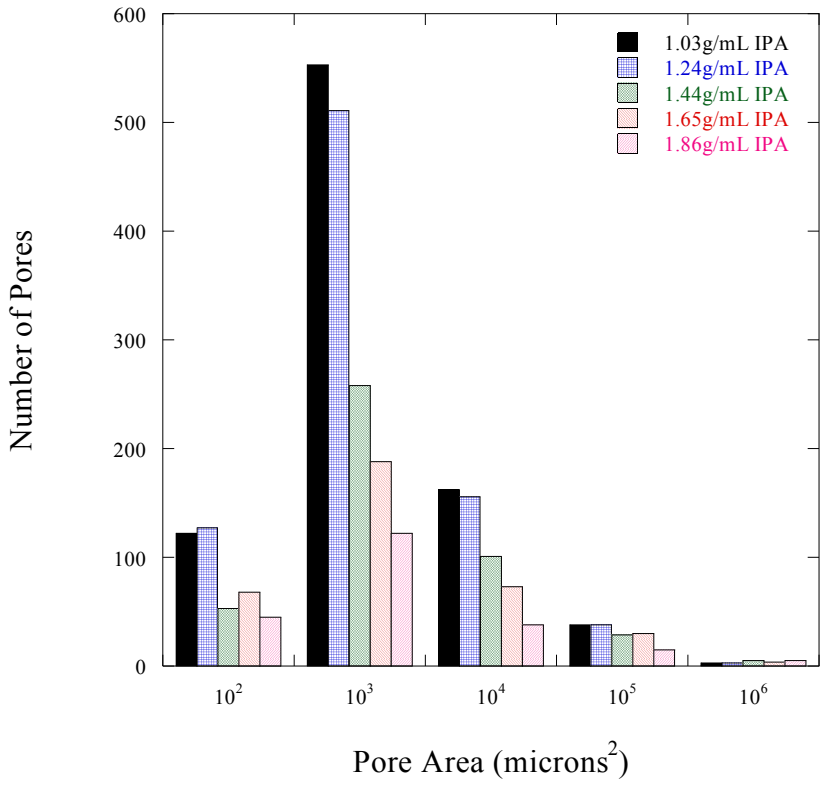

Figure 25. Pore size distribution generated from SEM micrographs of foam samples prepared with a constant sugar concentration of 5.15g/mL**.** A lower isopropanol concentration will lead to more pores in the 10^3 micron^2 bin.

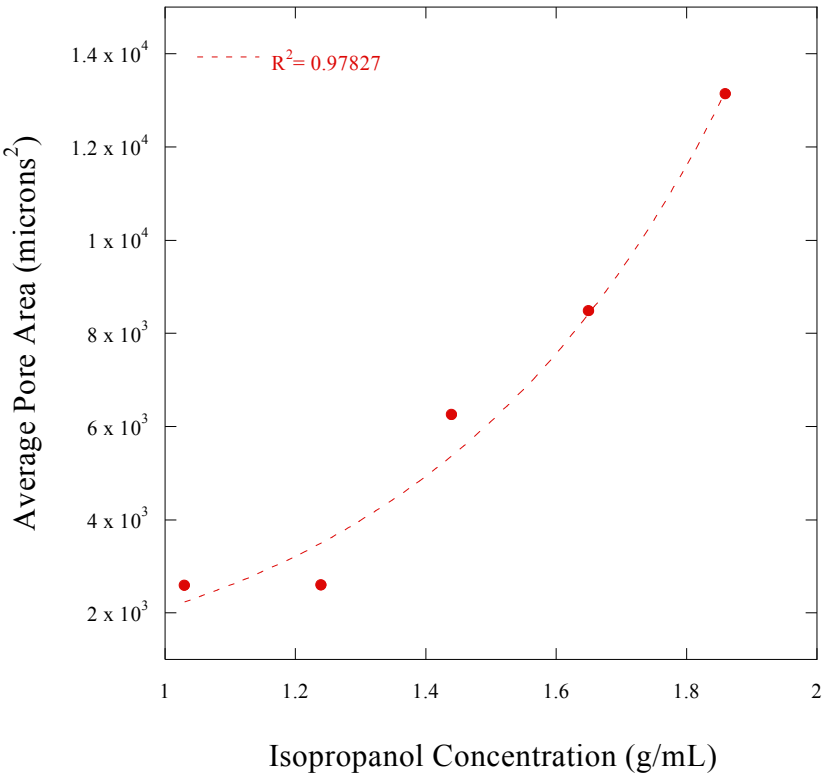

Figure 26. Average pore area generated from SEM micrographs of foam samples fabricated with a constant sugar concentration of 5.15g/mL. The average pore area increases with an increase in the isopropanol concentration. The data is fitted to an exponential equation with an R^2 value of 0.97827.

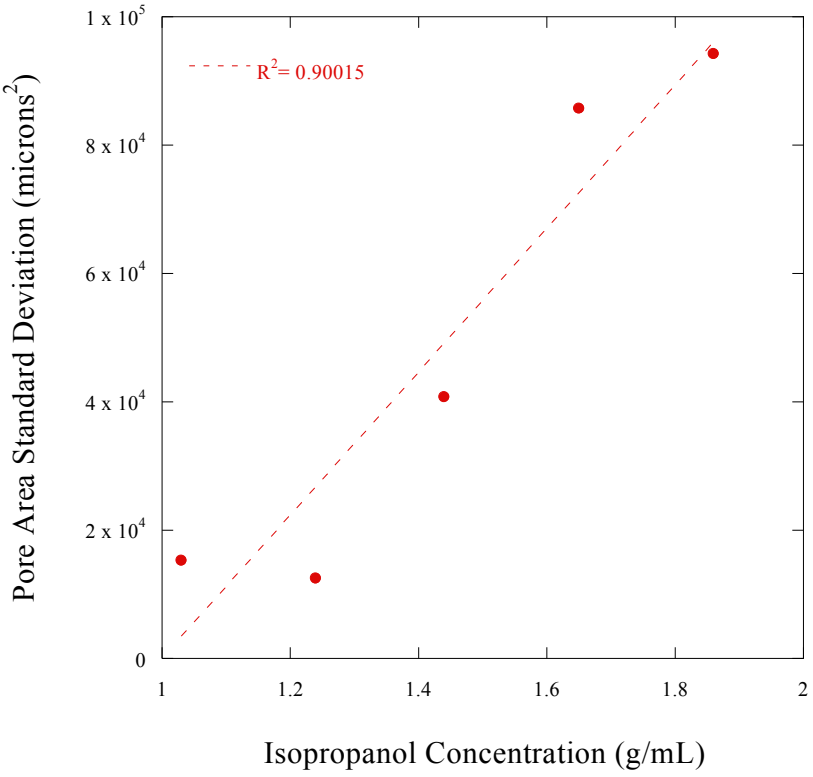

Figure 27. Pore area standard deviation generated from SEM micrographs of foam samples fabricated with a constant sugar concentration of 5.15g/mL. The standard deviation of the pore area increases with the isopropanol concentration, indicating that the pores become less uniform with an increase in the isopropanol concentration. The data is fitted to a line with a R^2 value of 0.90015.

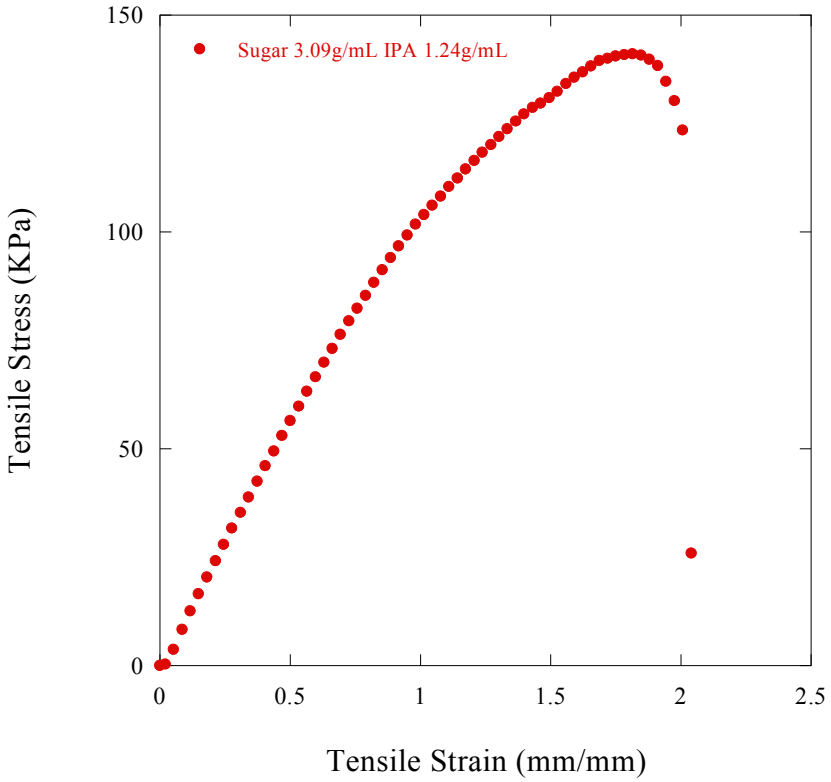

Figure 28. An example of a graph of the raw data from the Instron tensile test machine. Foam samples were tested until failure. The UTS is the peak values of stress attained before sample failure.

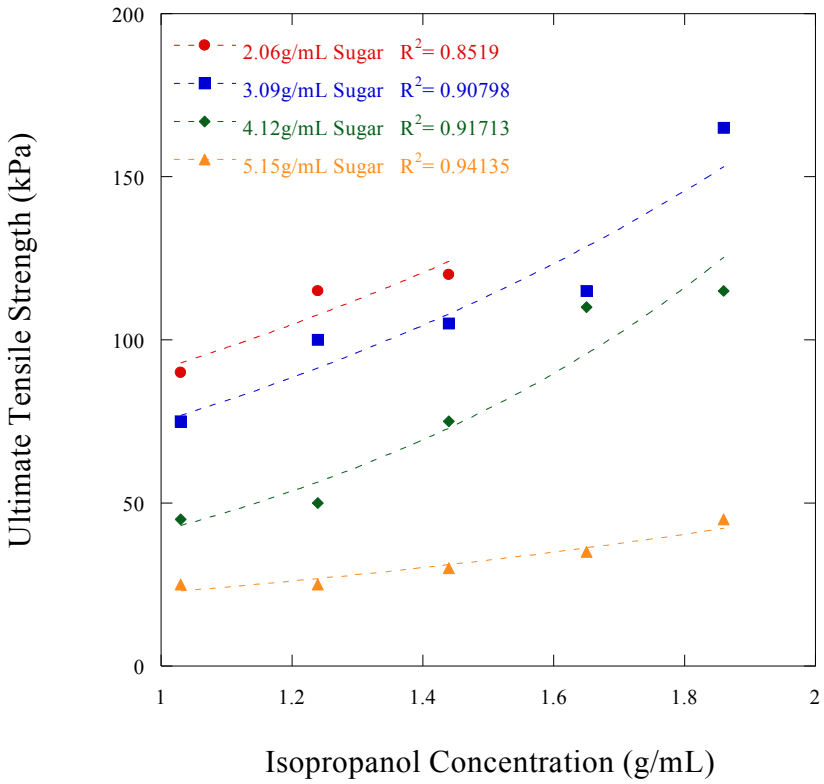

Figure 29. Average of three Ultimate Tensile Strength (UTS) tests for each of the foam compositions. The UTS of the foam samples increases with increasing isopropanol concentration, but decreases with the addition of sugar. The UTS of bulk PDMS is 2.24MPa. The data is fitted to exponential functions with the displayed R^2 values.

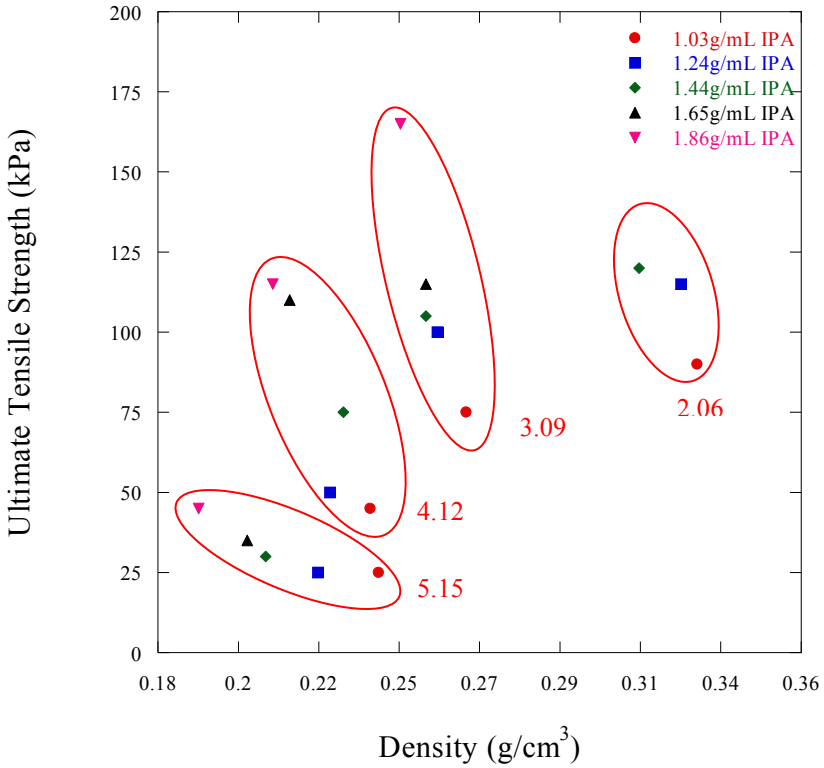

Figure 30. Groups of samples with a constant sugar concentration (in g/mL) are circled. Within each of these groups an increase in the isopropanol concentration not only leads to a decrease in the density of the foam, but also to an increase in the UTS.

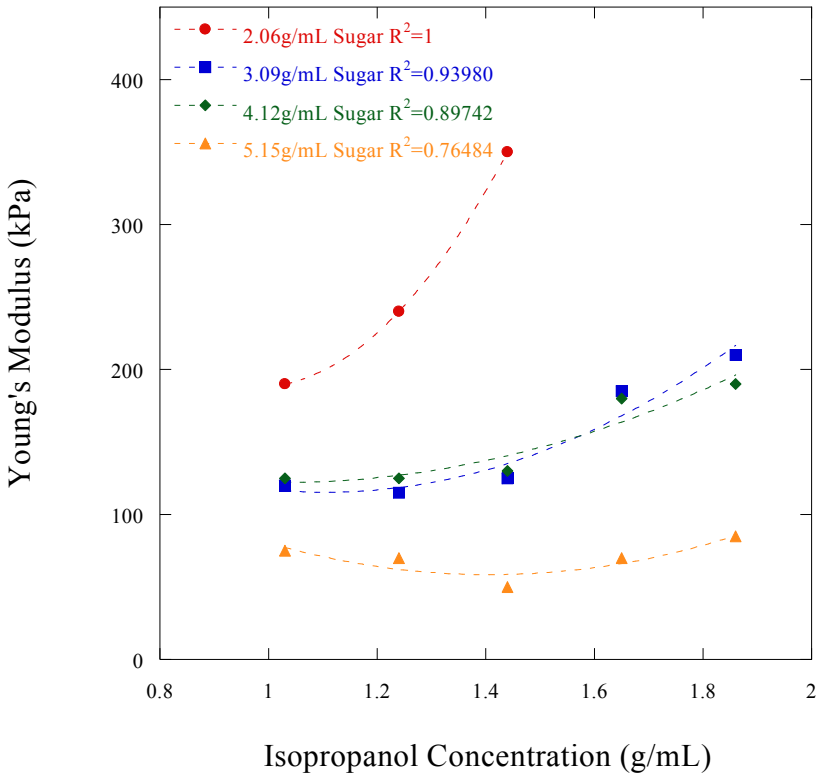

Figure 31. Average of the Young's Modulus of three samples for each composition**.** The Young's Modulus of the foam will increase drastically with an increase in the isopropanol concentration when there is a low sugar concentration in the suspo-emulsion, but when there is a higher concentration of sugar in the suspo-emulsion, the isopropanol concentration has less of an effect. The Young's Modulus of bulk PDMS ranges from 360KPa to 870KPa. The data is fitted to quadratic equations with the displayed R^2 values.

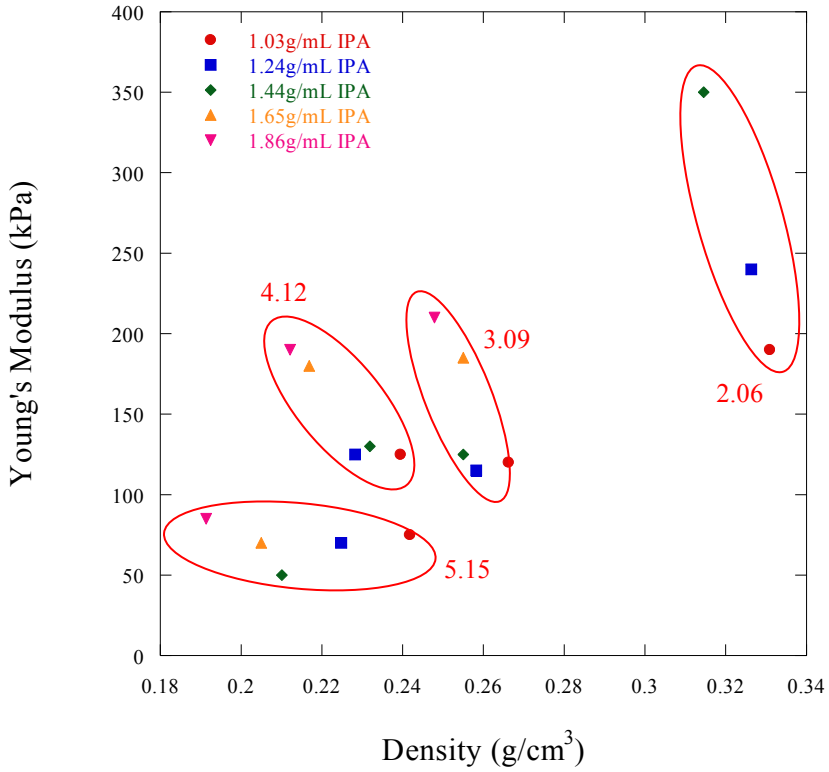

Figure 32. Groups of samples with constant sugar concentrations (in g/mL) are circled. Within each of these groups, an increase in the isopropanol concentration leads to a lower density, but also a higher Young's Modulus. The effect becomes less significant at higher sugar concentrations.

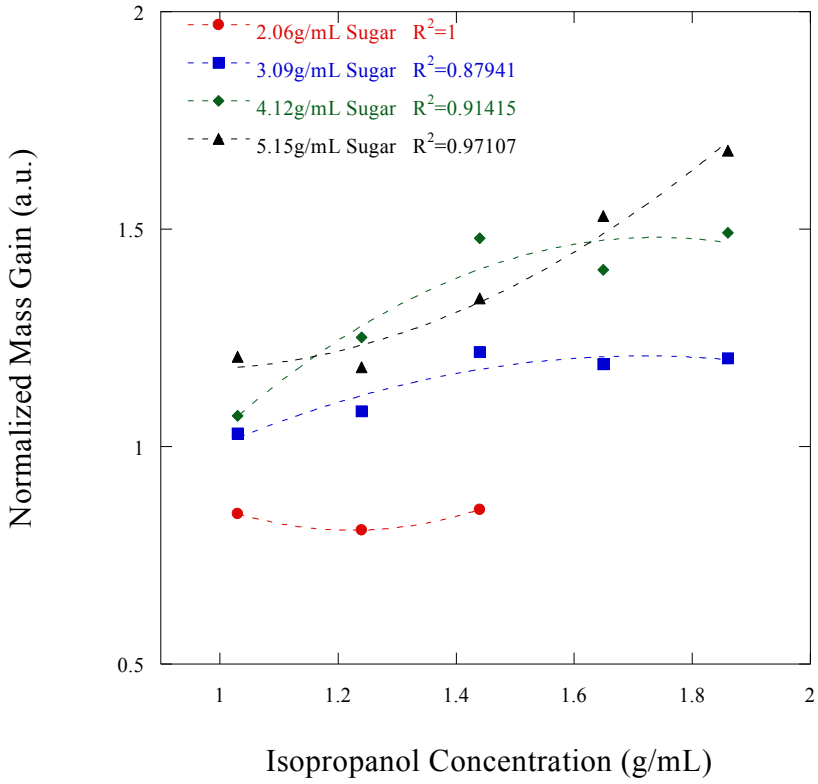

Figure 33. Normalized mass gains for foam samples placed on top of oil slick for 1 minute**.** Generally**,** more oil is absorbed by foam samples that were fabricated with higher isopropanol and sugar concentrations. The data is fitted to quadratic equations with the displayed R^2 values.

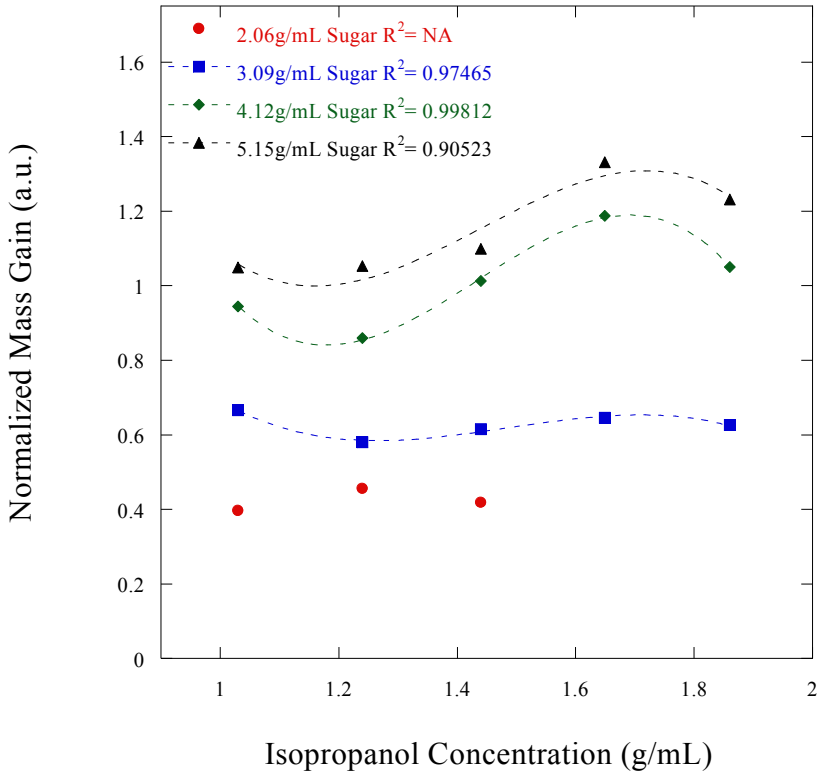

Figure 34. Normalized mass gains for foam samples placed on top of oil slick for 15 seconds**.** Oil absorption after 15 seconds shows a similar trend to the 1 minute experiment, but the normalized mass gains are lower. The data is fitted to cubic equations with the displayed R^2 values.

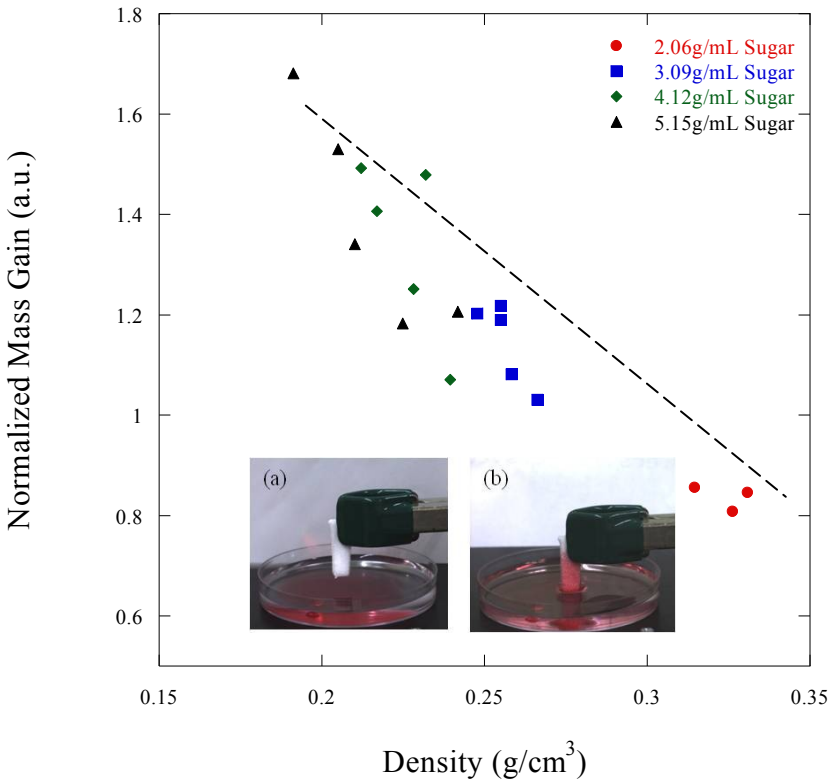

Figure 35. Normalized mass gains for foam samples placed on top of oil slick for 1 minute plotted against the density. The normalized mass gains appear inversely proportional to the density of the foam samples. Inset (a) is a picture of the foam before absorbing oil (dyed red for visualization) and (b) is after absorbing oil. The dotted line is to guide the reader.

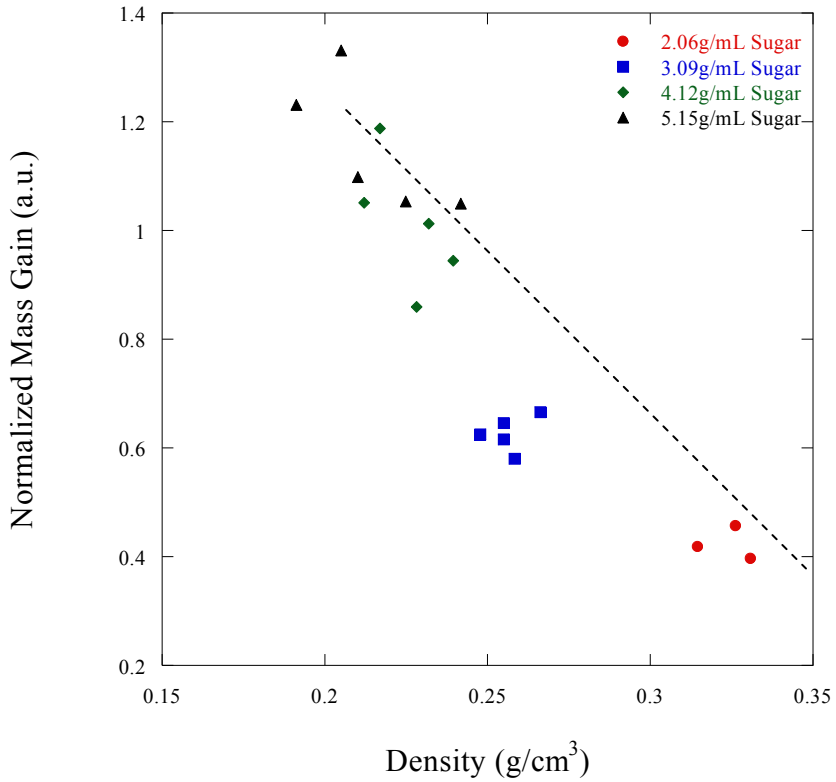

Figure 36. Normalized mass gains for foam samples placed on top of oil slick for 15 seconds plotted against the density. The normalized mass gains appear inversely proportional to the density of the foam samples and the data is more distinctively grouped by sugar concentration than the 1 minute trial. This is because for a shorter time interval, the flow rate of oil through the pores of the foam does not vary as much. The dotted line is to guide the reader.

Tables

25°C Slope is of the form A(t) + B

IPA (g/mL)	Sugar (g/mL)	A ($x10^{-7}$)	B ($x10^{-4}$)
1.03	3.09	-0.24	2.61
1.55	3.09	-3.24	6.37
1.03	4.12	-0.56	1.48
1.55	4.12	-3.9	5.40

38°C

IPA (g/mL)	Sugar (g/mL)	A ($x10^{-7}$)	B ($x10^{-4}$)
1.03	3.09	-10.00	12.12
1.55	3.09	-11.26	14.71
1.03	4.12	-1.52	4.35
1.55	4.12	-1.44	4.95

Table 1. Quadratic equations were fitted to the normalized bubble growth equations. These are the tabulated first derivatives of those equations, which are the bubble growth rates.

References

1. Jones, J.R., L.M. Ehrenfried, and L.L. Hench, *Optimising bioactive glass scaffolds for bone tissue engineering.* Biomaterials, 2006. **27**(7): p. 964-973.
2. Darder, M., et al., *Progress in Bionanocomposite and Bioinspired Foams.* Advanced Materials, 2011. **23**(44): p. 5262-5267.
3. Sepulveda, P., J.R. Jones, and L.L. Hench, *Bioactive sol-gel foams for tissue repair.* Journal of Biomedical Materials Research, 2002. **59**(2): p. 340-348.
4. Yang, H.Q., et al., *Synthesis and catalytic performances of hierarchical SAPO-34 monolith.* Journal of Materials Chemistry, 2010. **20**(16): p. 3227-3231.
5. Scheffler, F., et al., *Zeolite covered polymer derived ceramic foams: novel hierarchical pore systems for sorption and catalysis.* Advances in Applied Ceramics, 2005. **104**(1): p. 43-48.
6. Barg, S., et al., *Novel open cell aluminum foams and their use as reactive support for zeolite crystallization.* Journal of Porous Materials, 2011. **18**(1): p. 89-98.
7. Rainer, A., et al., *Foaming of filled polyurethanes for fabrication of porous anode supports for intermediate temperature-solid oxide fuel cells.* Journal of the American Ceramic Society, 2006. **89**(6): p. 1795-1800.
8. Brun, N., et al., *Design of Hierarchical Porous Carbonaceous Foams from a Dual-Template Approach and Their Use as Electrochemical Capacitor and Li Ion Battery Negative Electrodes.* Journal of Physical Chemistry C, 2012. **116**(1): p. 1408-1421.
9. Verdejo, R., et al., *Enhanced acoustic damping in flexible polyurethane foams filled with carbon nanotubes.* Composites Science and Technology, 2009. **69**(10): p. 1564-1569.
10. Scarpa, F., L.G. Ciffo, and J.R. Yates, *Dynamic properties of high structural integrity auxetic open cell foam.* Smart Materials & Structures, 2004. **13**(1): p. 49-56.
11. Kuhn, J., et al., *Thermal Transport in Polystyrene and Polyurethan Foam Insulations.* International Journal of Heat and Mass Transfer, 1992. **35**(7): p. 1795-1801.
12. Hrubesh, L.W. and R.W. Pekala, *Thermal Properties of Organic and Inorganic Aerogels.* Journal of Materials Research, 1994. **9**(3): p. 731-738.
13. Chen, J., H. Park, and K. Park, *Synthesis of superporous hydrogels: Hydrogels with fast swelling and superabsorbent properties.* Journal of Biomedical Materials Research, 1999. **44**(1): p. 53-62.
14. Tondi, G., et al., *Tannin-based rigid foams: A survey of chemical and physical properties.* Bioresource Technology, 2009. **100**(21): p. 5162-5169.
15. Cameron, N.R., *High internal phase emulsion templating as a route to well-defined porous polymers.* Polymer, 2005. **46**(5): p. 1439-1449.
16. Eaves, D., *Handbook of Polymer Foams.* 2004.
17. Wong, L.L.C., et al., *Macroporous Polymers with Hierarchical Pore Structure from Emulsion Templates Stabilised by Both Particles and Surfactants.*

Macromolecular Rapid Communications, 2011. **32**(19): p. 1563-1568.
18. Tariq, F., et al., *The influence of nanoscale microstructural variations on the pellet scale flow properties of hierarchical porous catalytic structures using multiscale 3D imaging.* Chemical Engineering Science, 2011. **66**(23): p. 5804-5812.
19. Wang, X.S. and R. Xia, *Size-dependent effective modulus of hierarchical nanoporous foams.* Epl, 2010. **92**(1).
20. Wei, G. and P.X. Ma, *Macroporous and nanofibrous polymer scaffolds and polymer/bone-like apatite composite scaffolds generated by sugar spheres.* Journal of Biomedical Materials Research Part A, 2006. **78A**(2): p. 306-315.
21. Vaquette, C., et al., *An innovative method to obtain porous PLLA scaffolds with highly spherical and interconnected pores.* Journal of Biomedical Materials Research Part B-Applied Biomaterials, 2008. **86B**(1): p. 9-17.
22. Choi, S.J., et al., *A Polydimethylsiloxane (PDMS) Sponge for the Selective Absorption of Oil from Water.* Acs Applied Materials & Interfaces, 2011. **3**(12): p. 4552-4556.
23. Hou, Q.P., D.W. Grijpma, and J. Feijen, *Preparation of interconnected highly porous polymeric structures by a replication and freeze-drying process.* Journal of Biomedical Materials Research Part B-Applied Biomaterials, 2003. **67B**(2): p. 732-740.
24. Yang, Y.F., et al., *Formation of porous PLGA scaffolds by a combining method of thermally induced phase separation and porogen leaching.* Journal of Applied Polymer Science, 2008. **109**(2): p. 1232-1241.
25. Narayan, D. and S.S. Venkatraman, *Effect of pore size and interpore distance on endothelial cell growth on polymers.* Journal of Biomedical Materials Research Part A, 2008. **87A**(3): p. 710-718.
26. Misra, S.K., et al., *Poly(3-hydroxybutyrate) multifunctional composite scaffolds for tissue engineering applications.* Biomaterials, 2010. **31**(10): p. 2806-2815.
27. Luckarift, H.R., et al., *Facile Fabrication of Scalable, Hierarchically Structured Polymer/Carbon Architectures for Bioelectrodes.* Acs Applied Materials & Interfaces, 2012. **4**(4): p. 2082-2087.
28. Dorati, R., et al., *Effect of porogen on the physico-chemical properties and degradation performance of PLGA scaffolds.* Polymer Degradation and Stability, 2010. **95**(4): p. 694-701.
29. Makaya, K., et al., *Comparative study of silk fibroin porous scaffolds derived from salt/water and sucrose/hexafluoroisopropanol in cartilage formation.* Journal of Bioscience and Bioengineering, 2009. **108**(1): p. 68-75.
30. Huang, Y.C., et al., *Fabrication and in vitro testing of polymeric delivery system for condensed DNA.* Journal of Biomedical Materials Research Part A, 2003. **67A**(4): p. 1384-1392.
31. Gong, X.H., et al., *Fabrication of graded macroporous poly(lactic acid) scaffold by a progressive solvent casting/porogen leaching approach.* Journal of Applied Polymer Science, 2012. **125**(1): p. 571-577.
32. Tran, R.T., et al., *A new generation of sodium chloride porogen for tissue engineering.* Biotechnology and Applied Biochemistry, 2011. **58**(5): p. 335-344.
33. Ghosh, S., et al., *The double porogen approach as a new technique for the fabrication of interconnected poly(L-lactic acid) and starch based biodegradable*

scaffolds. Journal of Materials Science-Materials in Medicine, 2007. **18**(2): p. 185-193.
34. Lin, H.R., et al., *Preparation of macroporous biodegradable PLGA scaffolds for cell attachment with the use of mixed salts as porogen additives.* Journal of Biomedical Materials Research, 2002. **63**(3): p. 271-279.
35. Lin-Gibson, S., et al., *Systematic investigation of porogen size and content on scaffold morphometric parameters and properties.* Biomacromolecules, 2007. **8**(5): p. 1511-1518.
36. Kim, T.G., H.J. Chung, and T.G. Park, *Macroporous and nanofibrous hyaluronic acid/collagen hybrid scaffold fabricated by concurrent electrospinning and deposition/leaching of salt particles.* Acta Biomaterialia, 2008. **4**(6): p. 1611-1619.
37. Thomson, R.C., et al., *Hydroxyapatite fiber reinforced poly(alpha-hydroxy ester) foams for bone regeneration.* Biomaterials, 1998. **19**(21): p. 1935-1943.
38. Murphy, W.L., et al., *Salt fusion: An approach to improve pore interconnectivity within tissue engineering scaffolds.* Tissue Engineering, 2002. **8**(1): p. 43-52.
39. Cai, Q., et al., *A novel porous cells scaffold made of polylactide-dextran blend by combining phase-separation and particle-leaching techniques.* Biomaterials, 2002. **23**(23): p. 4483-4492.
40. Lee, S.H., et al., *Thermally produced biodegradable scaffolds for cartilage tissue engineering.* Macromolecular Bioscience, 2004. **4**(8): p. 802-810.
41. Kohnke, T., et al., *Nanoreinforced xylan-cellulose composite foams by freeze-casting.* Green Chemistry, 2012. **14**(7): p. 1864-1869.
42. Mao, M., et al., *Ice-template-induced silk fibroin–chitosan scaffolds with predefined microfluidic channels and fully porous structures.* Acta Biomaterialia, 2012. **8**(6): p. 2175-2184.
43. Li, J.S., et al., *A one-step method to fabricate PLLA scaffolds with deposition of bioactive hydroxyapatite and collagen using ice-based microporogens.* Acta Biomaterialia, 2010. **6**(6): p. 2013-2019.
44. Martins, L., et al., *Preparation of hierarchically structured porous aluminas by a dual soft template method.* Microporous and Mesoporous Materials, 2010. **132**(1-2): p. 268-275.
45. Texter, J., *Templating hydrogels.* Colloid and Polymer Science, 2009. **287**(3): p. 313-321.
46. Binks, B.P., *Particles as surfactants - similarities and differences.* Current Opinion in Colloid & Interface Science, 2002. **7**(1-2): p. 21-41.
47. Binks, B.P. and R. Murakami, *Phase inversion of particle-stabilized materials from foams to dry water.* Nature Materials, 2006. **5**(11): p. 865-869.
48. Binks, B.P. and T.S. Horozov, *Aqueous foams stabilized solely by silica nanoparticles.* Angewandte Chemie-International Edition, 2005. **44**(24): p. 3722-3725.
49. Joanna C. H. Wong, E.T., Stephan Busato, Urs T. Gonzenbach, Andre R. Studart, Paolo Ermanni and Ludwig J. Gaucklerb, *Designing macroporous polymers from particle-stabilized foams.* Journal of Materials Chemistry, 2010. **20**(27).
50. S.J. Clarson, J.A.S., *Siloxane Polymers*. 1993, Englewood Cliffs, NJ: Prentice-Hall.
51. Carn, F., et al., *Three-dimensional opal-like silica foams.* Langmuir, 2006. **22**(12):

p. 5469-5475.
52. Mao, X.J., S.W. Wang, and S.Z. Shimai, *Porous ceramics with tri-modal pores prepared by foaming and starch consolidation.* Ceramics International, 2008. **34**(1): p. 107-112.
53. Suzuki, K., K. Ikari, and H. Imai, *Synthesis of mesoporous silica foams with hierarchical trimodal pore structures.* Journal of Materials Chemistry, 2003. **13**(7): p. 1812-1816.
54. Gross, A.F. and A.P. Nowak, *Hierarchical Carbon Foams with Independently Tunable Mesopore and Macropore Size Distributions.* Langmuir, 2010. **26**(13): p. 11378-11383.
55. Studart, A.R., et al., *Hierarchical Porous Materials Made by Drying Complex Suspensions.* Langmuir, 2011. **27**(3): p. 955-964.
56. Juillerat, F.K., et al., *Self-setting particle-stabilized foams with hierarchical pore structures.* Materials Letters, 2010. **64**(13): p. 1468-1470.
57. Vakifahmetoglu, C., et al., *SiOC Ceramic Monoliths with Hierarchical Porosity.* International Journal of Applied Ceramic Technology, 2010. **7**(4): p. 528-535.
58. Huerta, L., et al., *Nanosized mesoporous silica coatings on ceramic foams: New hierarchical rigid monoliths.* Chemistry of Materials, 2007. **19**(5): p. 1082-1088.
59. Alauzun, J.G., et al., *Novel monolith-type boron nitride hierarchical foams obtained through integrative chemistry.* Journal of Materials Chemistry, 2011. **21**(36): p. 14025-14030.
60. Zhang, H., et al., *Preparation of TiO2, CeO2, and ZrO2 hierarchical structures in "one-pot" reactions.* Journal of Colloid and Interface Science, 2009. **333**(2): p. 764-770.
61. Cohen, M.J., *Economic Impact of an Environmental Accident - A Time-series Analysis of the Exxon Valdez Oil Spill in South-Central Alaska.* Sociological Spectrum, 1993. **13**(1): p. 35-63.
62. Dalton, T. and D. Jin, *Extent and frequency of vessel oil spills in US marine protected areas.* Marine Pollution Bulletin, 2010. **60**(11): p. 1939-1945.
63. Balk, L., et al., *Biomarkers in Natural Fish Populations Indicate Adverse Biological Effects of Offshore Oil Production.* Plos One, 2011. **6**(5).
64. Balseiro, A., et al., *Pathological features in marine birds affected by the prestige's oil spill in the north of Spain.* Journal of Wildlife Diseases, 2005. **41**(2): p. 371-378.
65. Dean, T.A., et al., *Food limitation and the recovery of sea otters following the 'Exxon Valdez' oil spill.* Marine Ecology-Progress Series, 2002. **241**: p. 255-270.
66. Ormseth, O.A. and M. Ben-David, *Ingestion of crude oil: effects on digesta retention times and nutrient uptake in captive river otters.* Journal of Comparative Physiology B-Biochemical Systemic and Environmental Physiology, 2000. **170**(5-6): p. 419-428.
67. Garrott, R.A., L.L. Eberhardt, and D.M. Burn, *Mortality of Sea Otters in Prince-William Sound Following the Exxon-Valdez Oil Spill.* Marine Mammal Science, 1993. **9**(4): p. 343-359.
68. Koyama, J. and A. Kakuno, *Toxicity of heavy fuel oil, dispersant, and oil-dispersant mixtures to a marine fish, Pagrus major.* Fisheries Science, 2004. **70**(4): p. 587-594.
69. Ford, G.S., *An investigation into the relationship of retail gas prices on oil*

company profitability. Applied Economics, 2011. **43**(27): p. 4033-4041.
70. Liu, X. and K.W. Wirtz, *The economy of oil spills: Direct and indirect costs as a function of spill size.* Journal of Hazardous Materials, 2009. **171**(1-3): p. 471-477.
71. *BP Establishes $20 Billion Dollar Claims Fund For Deepwater Horizon Spill and Outlines Dividend Decisions*. 2010 June.
72. *Winning Teams Announced in the $1.4 Million Wendy Schmidt oil cleanup X Challenge*. 2012.
73. Najar, A.M. and J.T. Turner, *Enhanced oil recovery using the rotating-disc skimmer.* Proceedings of the Institution of Mechanical Engineers Part E-Journal of Process Mechanical Engineering, 2000. **214**(E4): p. 271-282.
74. Fountain, H., *Advances in Oil Spill Cleanup Lag Since Valdez*, in *New York Times*. 2010.
75. Petrucci, J., *When to Use an Oil Skimmer.* Power, 2010. **154**(1): p. 17-18.
76. Nordvik, A.B., *The Technology Windows of Opportunity for Marine Oil Spill Response as Related to Oil Weathering and Operations.* Spill Science & Technology Bulletin, 1995. **2**(1): p. 17-46.
77. Nordvik, A.B., et al., *Oil and water separation in marine oil spill clean-up operations.* Spill Science & Technology Bulletin, 1996. **3**(3): p. 107-122.
78. Lee, K. and S. de Mora, *In situ bioremediation strategies for oiled shoreline environments.* Environmental Technology, 1999. **20**(8): p. 783-794.
79. Berninger, J.P., E.S. Williams, and B.W. Brooks, *An Initial Probabilistic Hazard Assessment of Oil Dispersants Approved by the United States National Contingency Plan.* Environmental Toxicology and Chemistry, 2011. **30**(7): p. 1704-1708.
80. Reynolds, J.G., P.R. Coronado, and L.W. Hrubesh, *Hydrophobic aerogels for oil-spill cleanup - Intrinsic absorbing properties.* Energy Sources, 2001. **23**(9): p. 831-843.
81. Cai, J.C., Y; Luo, J; Sears, C. *Utilizing Porous Materials for Oil Spill Cleanup*. 2010.
82. Annunciado, T.R., T.H.D. Sydenstricker, and S.C. Amico, *Experimental investigation of various vegetable fibers as sorbent materials for oil spills.* Marine Pollution Bulletin, 2005. **50**(11): p. 1340-1346.